2013-01-01

Determination Of The Effects Of ZnO And CeO2 Nanoparticles In Mesquite (Prosopis Juliflora) And Soybean (Glycine Max): Synchrotron And Spectroscopic Approaches

Jose Angel Hernandez Viezcas
University of Texas at El Paso, jahernandez19@miners.utep.edu

DETERMINATION OF THE EFFECTS OF ZnO AND CeO_2 NANOPARTICLES IN MESQUITE (PROSOPIS JULIFLORA) AND SOYBEAN (GLYCINE MAX): SYNCHROTRON AND SPECTROSCOPIC APPROACHES

JOSE ANGEL HERNANDEZ-VIEZCAS

Department of Chemistry

APPROVED:

Jorge Gardea-Torresdey, Ph.D., Chair

Mahesh Narayan, Ph.D.

Jose Peralta-Videa, Ph.D.

Chintalapalle Ramana, Ph.D.

Benjamin C. Flores, Ph.D.
Dean of the Graduate School

Dedication

This work is dedicated to my family. My deepest love and admiration to my father my mother and my sister, for your never ending love. This work is also dedicated to my wife and my son, who are the joy of my life.

DETERMINATION OF THE EFFECTS OF ZnO AND CeO2 NANOPARTICLES IN MESQUITE (PROSOPIS JULIFLORA) AND SOYBEAN (GLYCINE MAX): SYNCHROTRON AND SPECTROSCOPIC STUDIES

by

JOSE ANGEL HERNANDEZ-VIEZCAS, M.S

DISSERTATION

Presented to the Faculty of the Graduate School of

The University of Texas at El Paso

in Partial Fulfillment

of the Requirements

for the Degree of

DOCTOR OF PHILOSOPHY

Department of Chemistry

THE UNIVERSITY OF TEXAS AT EL PASO

December 2013

Acknowledgements

The University of Texas at El Paso has given me a unique education and a new future for me and my family, I will always be grateful to this institution. First and foremost, I would like to show my gratitude to Dr. Jorge Gardea-Torresdey, a mentor that goes the extra step to help his students. Thank you for giving me the opportunity to work under your mentorship, my deepest appreciation for all you have taught me academically and in my personal life and for being a figure we can look up to. I would also like to thank Dr. Peralta for his support, and valuable ideas throughout 6 years of friendship. I would also like thank Dr. Narayan, I always appreciate your advice and smart comments. Dr. Ramana, thank you for accepting the task of being in my dissertation committee and thank you for your advice. Throughout, my time at UTEP I had been very fortunate to come in contact with persons that have enriched my life. I would like to acknowledge Dr. Laura-Lopez and Dr. Guadalupe de la Rosa from whom I have learn to be a better scientist and a better person. Special appreciation to my friend Dr. Hirman Castillo-Michel, thank you for all your help and for introducing me to the world of synchrotron radiation. I would also like to thank Alia Servin and Dr. Lijuan Zhao for all the help and friendship.

I would like to show my gratitude to the Gardea-Torresday research group, thank you for being another family for me and thank you for all your help. Lastly, I acknowledge my family, you have always supported and encouraged me to carry on, and you fill my everyday life with happiness. I also acknowledge National Science Foundation and the Environmental Protection Agency for the funding under Cooperative Agreement Number DBI-0830117 and the Consejo Nacional de Ciencia y Tecnologia of Mexico (CONACyT) for its financial support.

.

Abstract

The rapid growth of nanotechnology is exposing the environment to abnormal concentrations of engineered nanoparticles (NPs). There is concern about the unknown consequences of NPs on the environment and human health. This dissertation has relied significantly on Synchrotron and other spectroscopic techniques to give insights on the effects, speciation and distribution of two metal oxide nanoparticles (ZnO, CeO2) on two plant species (Mesquite and Soybean). We evaluated the effects of ZnO (10 nm) and CeO2 (8 nm) NPs on a plant species native to the semi-arid regions of North America, Mesquite (Prosopis juliflora velutina). Mesquite plants grown in hydroponic culture with ZnO NPs presented an increased uptake of Zn when compared to control plants. Zn synchrotron μXRF from root transversal sections (30 μm) showed Zn accumulated mainly in the vascular region. Zn μXRF maps obtained from the leaves showed that Zn is mainly concentrated in the veins. Combined Bulk and μXANES synchrotron analysis showed that Zn has different coordination environments compared to the ZnO NPs, and corroborated that ZnO NPs were transformed on/in the root surface and transported as Zn (II) from roots to leaves. Exposure to ZnO NPs increased the specific activity of stress enzymes catalase in root, stem and leaves and ascorbate peroxidase only in stem and leaves. The concentration of Ce in mesquite plants exposed to CeO2 NPs was higher when compared to the control; however Ce μXRF maps showed most of the cerium was adsorbed in the root. Bulk XANES showed that Ce maintained the same coordination as the CeO_2 NPs.

Few reports thus far have addressed the entire life cycle of plants grown in NP-contaminated soil. We performed a lifecycle study of ZnO and CeO_2 NPs with the fifth largest crop produced in the world and second in the USA, Soybean (Glycine max).We determined the effects of NPs exposure and the potential storage of NPs or their biotransformed products in edible/reproductive organs of the plants in order to study the possible transfer of NPs into the food chain and potentially into the next plant generation.

Soybean (Glycine max) seeds were germinated and grown to full maturity in organic farm soil amended with either ZnO NPs or CeO2 NPs at different concentrations. At harvest, synchrotron μ-XRF and μ-XANES analyses were performed on soybean tissues, including pods, to determine the forms of

Ce and Zn in NP-treated plants. The X-ray absorption spectroscopy studies showed no presence of ZnO NPs within tissues. However, μ-XANES data showed O-bound Zn, in a form resembling Zn-citrate, which could be an important Zn complex in the soybean grains. On the other hand, the synchrotron μ-XANES results showed that Ce remained mostly as CeO2 NPs within the plant. Our results also showed that a small percentage of Ce(IV), the oxidation state of Ce in CeO2 NPs, was biotransformed to Ce(III). Our results also showed that the plants exposed to CeO2 diminished in growth but most importantly, nitrogen fixation was stopped at higher exposure concentrations. To our knowledge, this is the first report on the presence and effects of CeO2 and Zn compounds in the reproductive/edible portion of the soybean plant grown in farm soil with CeO2 and ZnO NPs.

Table of Contents

List of Tables

List of Figures

CHAPTER 1

Introduction

An increasing production and use of nano-sized materials has raised concerns about their possible impacts on the environment and human health. Although there is no accepted international definition, it is generally accepted that Nanoparticles (NPs) are materials having one or more dimension of the order of 100 nm or less.[1] Due to their small size, nanoparticles (NPs) escape the laws of Newtonian physics since they don't behave like solids, liquids or gases.[2] The ability to manipulate NPs along with their unique properties has given rise to the thriving field of nanotechnology. Nanotechnology has increased so quickly that, by the year 2000, over 60 countries had established national programs on nanotechnology. One trillion dollars' worth of nanotechnology-based products is expected on the market by the year 2015, representing a 500 % increase from 2008.[3] Figure 1 shows the number of products that disclose NPs in their composition, these 1600 goods are already being produced, sold and commercially used as of 2013.[4]

Zinc oxide (ZnO) and cerium dioxide (CeO_2, nanoceria) NPs are among the most highly utilized NPs in industry.[5] ZnO NPs are widely used in sunscreen products, as gas sensors[6], anti-bacterial agents[7], optical and electrical devices[8], and as pigments[9]. On the other hand, the high oxygen storage capacity of nanoceria makes it an excellent catalyst for internal combustion and oil cracking processes.[10,11] In addition, nanoceria is also used for gas sensors[12], sunscreen, and cosmetic creams[13].

However, after end-user applications, these products and residues will find their way into the environment, potentially reaching agricultural soils through biosolids, and other routes[14]. Moreover, ZnO and CeO_2 NPs are potentially toxic to humans[15,16].

Risk assessment and nanotoxicological studies have been performed on a few model crop plants and have included only the germination process and first growth stage of the plants[17-19]. As highlighted in a recent review, our knowledge of plant nanotoxicology is in its infancy, and more studies are needed to fully understand the effects of NPs in plants. Furthermore, very few studies have documented the biotransformation of NPs in vegetative tissues within plants, and there is a lack of information on the biotransformation of NPs in mature crops[20].

This dissertation relies on Synchrotron and other spectroscopic techniques to give insights on the effects, speciation and distribution of two metal oxide NPs (ZnO, CeO2) on two plant species (*Prosopis juliflora velutina* and *Glycine max*).

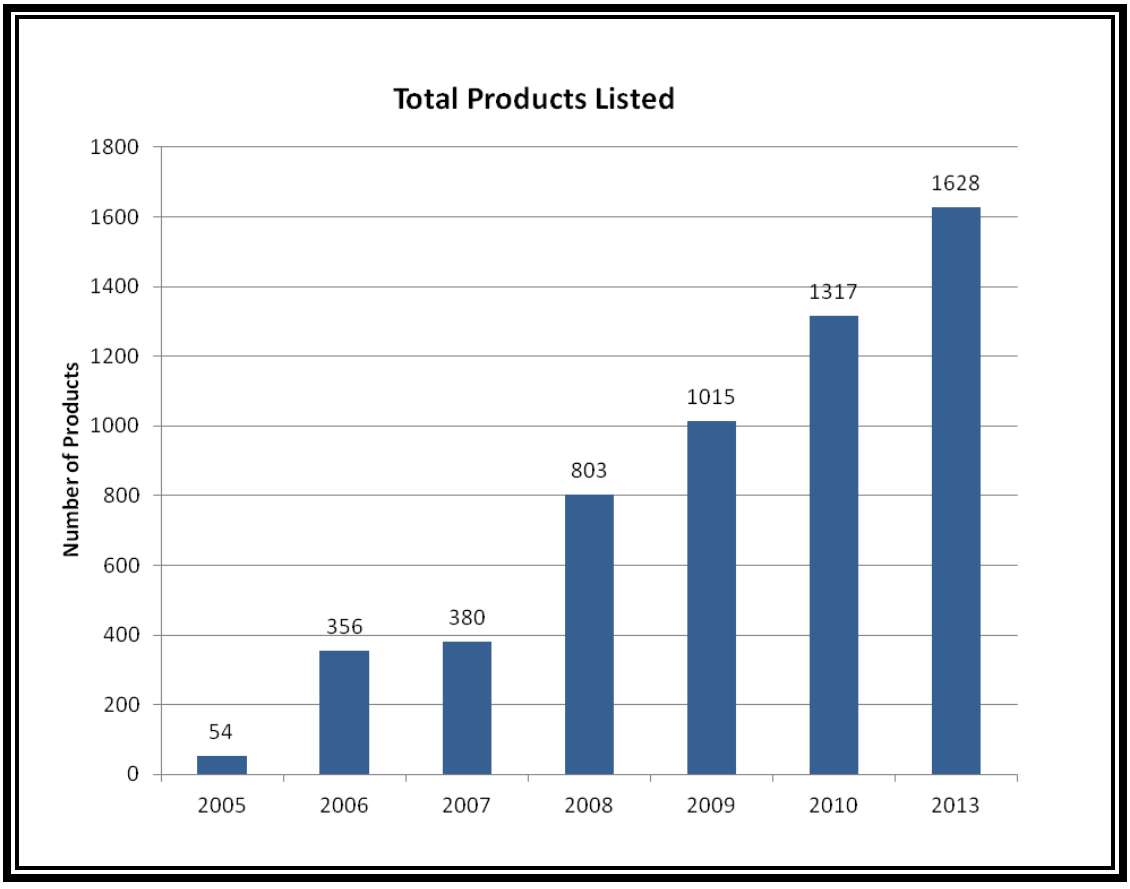

Figure 1: Number of total products on the market containing nanoparticles expressed by year.[4]

1.1 SYNCHROTRON RADIATION TECHNIQUES

Synchrotron origins can be traced to equipment originally developed for high energy or nuclear physics. The first observation of synchrotron light was made on 70-MeV electron synchrotron at the General Electric Research Laboratory in Schenectady, New York, on April 24, 1947.[21] The machine was not shielded to allow technicians to check with a mirror for sparks, that day the group saw a bright arc of light, which the physicist realized was coming from the electron beam. The first generation of synchrotron light sources was also called parasitic facilities since physicists in charge of high energy research centers considered the emission of radiation a loss in the particle energy.

Today, third generation synchrotrons accelerate electrons in a linear accelerator and then in a booster ring to nearly the speed of light. Afterwards, the electrons are transferred into a storage ring, where magnets force them into a curved trajectory. As electrons are forced in the circular path they emit the electromagnetic spectrum from infrared to x rays. Specialized optic devices direct the synchrotron radiation (SR) to experimental stations or beamlines. The ability to tune the energy and the brightness of SR makes synchrotron lightsources a unique facility. SR is hundreds of thousands times brighter than that from conventional X-ray tubes and with the use of monochromators the emitted light can be tuned to every need.[21]

1.2 X-Ray Absorption and Fluorescence

The basis for x-ray absorption spectroscopy (XAS) is the photo-electric effect, in which a photon is absorbed by an electron in a quantum core level of an atom. In order to remove the electron from its quantum level the x-ray incident energy must be higher than its binding energy, any excess incident energy will be transferred to a photo-electron that is ejected from the atom. Every element has a well defined core electron binding energy. SR can discriminate the desired element by tuning the x-ray energy to the suitable absorption edge. After x-rays are absorbed, the atom is in an excited state with a core hole and a photo-electron. There are two main mechanisms

for the relaxation of an exited state. The first one, is x-ray fluorescence (XRF) (Figure 2), in which a higher energy electron fills the original core hole, ejecting a photon of characteristic energy.[22] The energies emitted in the fluorescence phenomena can be used to identify the elements in a system. The second process for the relaxation of the excited state is the Auger effect, in which an electron falls from a higher energy level and a second electron is emitted out of the sample. Commonly, the XAS technique requires high photon fluxes and tunability that are only achievable in synchrotron light sources. Some of the advantages that XAS analysis provide include: a) information about the oxidation state, b) coordination environment of the analyte of interest, c) three-dimensional geometry and d) the ability of to analyze both crystalline and amorphous samples. The XAS spectrum can be divided in two energy regions, the first, X-ray absorption near edge structure (XANES) which encompass the pre edge region to 50 eV above the absorption edge (Figure 3). The second region is extended x-ray absorption fine structure (EXAFS); this region is due to quantum interference given by the back-scattering of the photoelectron from neighboring atoms.

Resonance signatures that are originated by the photoelectrons represent the main XANES features. The position of the edge increases with each electron that is removed from the valence shell by 1-3 eV. Furthermore, the absorption edge is affected by the bonding environment of the atom that absorbs the x-ray. Therefore XANES provides valuable information about the oxidation state and coordination of the element of interest. [23] The application of synchrotron techniques in plant sciences has been the subject of several reviews.[24-27] By using SR as the excitation source, materials can be analyzed with little or no pretreatment, therefore plants can be analyzed in their natural hydrated state. Another benefit from this technology is the capacity of multi-elemental analysis and the potential to combine different and complementary techniques.[28]

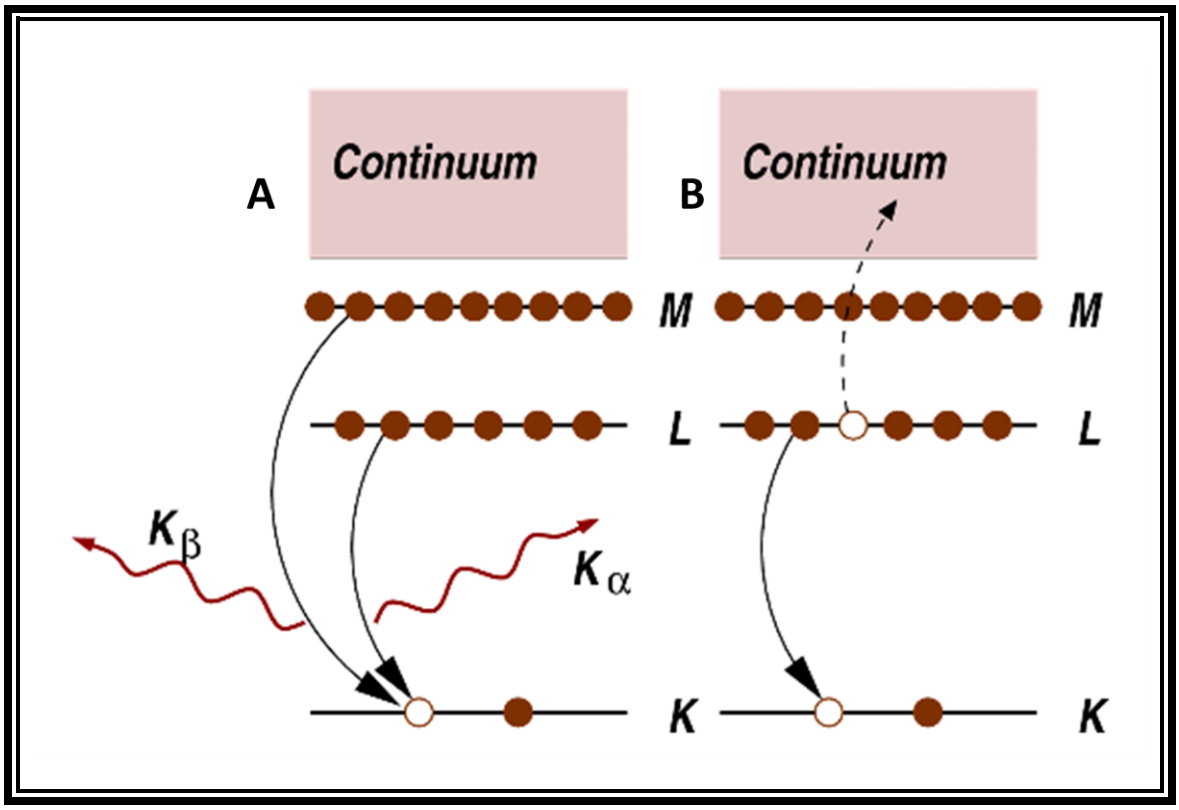

Figure 2: Decay of the excited state: x-ray fluorescence (A) and the Auger effect (B).[23]

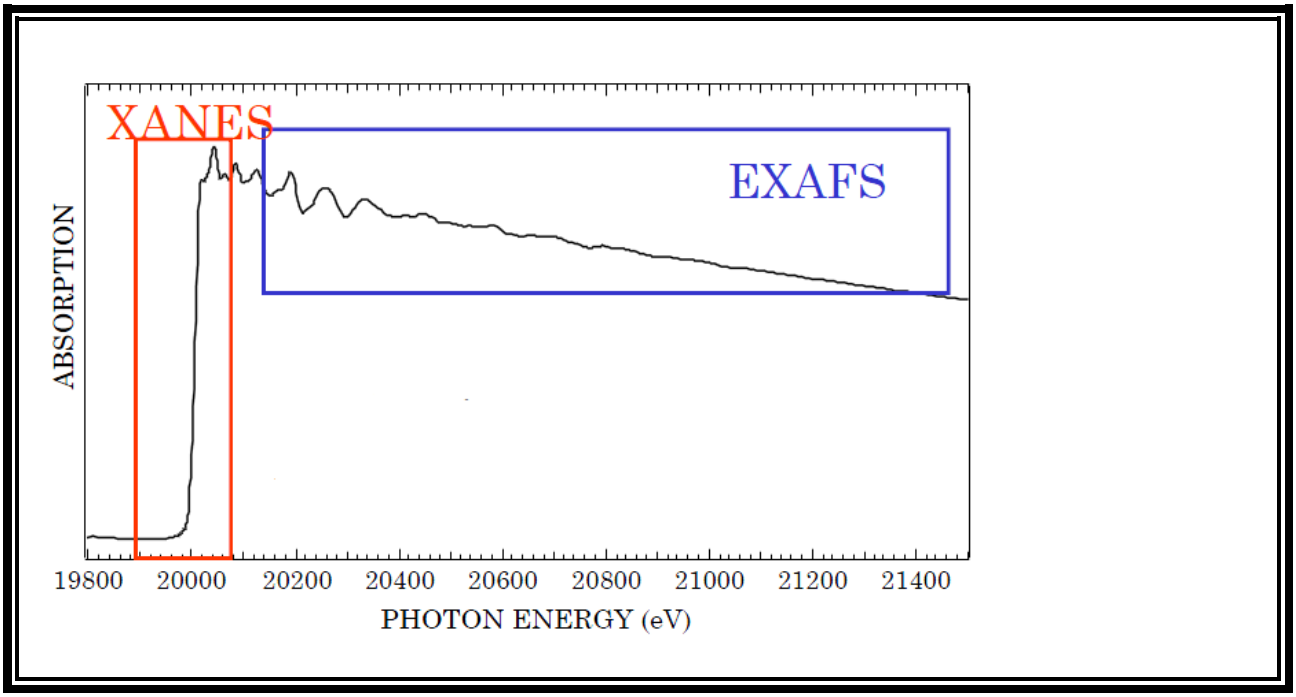

Figure 3: X-ray absorption spectrum of molybdenum metal from 19.8 to 21.5 keV showing the XANES and EXAFS regions.[23]

1.3 Research Objectives

The general objective of this research is:

To evaluate the effects of CeO2 and ZnO NPs on mesquite (Prosopis juluflora velutina) and soybean (Glicine Max) plants.

Mesquite specific objectives are:

1. Determine if the nanoceria and ZnO NPs are absorbed by mesquite grown at an early growth stage.
2. Determine if the NPs translocate throughout the plant.
3. Determine if the NPs remain in the same coordination state.
4. Determine the physiological effect of both NPs on mesquite.
5. Determine the mechanisms by which the plant up-takes the metal oxides.

Soybean specific objectives:

1. Determine if nanoceria and ZnO NPs can be absorbed and transocated to the fruit of the soybean.
2. Determine the mechanisms by which metal oxides are uptaken by the plant.
3. Determine the potential toxic effects to the plant
4. Determine the effects of NPs on plant nitrogen fixation.

CHAPTER 2

Spectroscopic verification of zinc absorption and distribution in the desert plant Prosopis juliflora-velutina (velvet mesquite) grown with ZnO nanoparticles

Abstract

The impact of metal nanoparticles (NPs) on biological systems, especially plants, is still not well

understood. The aim of this research was to determine the effects of zinc oxide (ZnO) NPs in velvet mesquite (Prosopis juliflora-velutina). Mesquite seedlings were grown for 15 days in hydroponics with ZnO NPs (10 nm) at concentrations varying from 500 to 4000 mg L-1. Zinc concentrations in roots, stems and leaves were determined by inductively coupled plasma optical emission spectroscopy (ICP-OES). Plant stress was examined by the specific activity of catalase (CAT) and ascorbate peroxidase (APOX); while the biotransformation of ZnO NPs and Zn distribution in tissues were determined by X-ray absorption spectroscopy (XAS) and micro X-ray fluorescence (μXRF), respectively. ICP-OES results showed that the highest Zn concentrations in tissues (2102±87, 1135±56, and 628±130 mg kg-1d wt in roots, stems, and leaves, respectively) were found at 2000 mg ZnO NPs L-1. Stress tests showed that ZnO NPs increased CAT in roots, stems, and leaves, while APOX increased only in stems and leaves. XANES spectra demonstrated that ZnO NPs were not present in mesquite tissues, while Zn was found as Zn(II), resembling the spectra of Zn(NO3)2. The μXRF analysis confirmed the presence of Zn in the vascular system of roots and leaves in ZnO NP treated plants.

2.1 Introduction

Little is known about the potential effects of NM on wild desert plants. Since they have acquired special characteristics to survive in harsh environments, it is hypothesized that plants from desert ecosystems will respond differently to NPs than plants in other ecosystems. Importantly, desert plants such as mesquite (Prosopis juliflora-velutina) improve soil structure and properties, and play an important role in the stability and conservation of other species[1].

Plants have special mechanisms to remove or inactivate reactive oxygen species (ROS) such as H_2O_2, OH-, and O_2- radicals that are byproducts of naturally occurring reactions. However, excess ROS can result in protein breakdown, lipid peroxidation in membranes, and DNA injury.[2] Previous studies have shown that heavy metals increased the activity of the antioxidant enzymes catalase (CAT) and ascorbate peroxidase (APOX) in plants.[3] However, there is lack of information on the effects of NPs upon ROS molecules. Lin et al.[4] reported a decrease in the superoxide dismutase activity (SOD) of Arabidopsis cells exposed to multiwalled carbon nanotubes (MWCNTs). In a study with rice cells treated with MWCNTs at 20 mg L, a significant time dependent induction was observed[5]. In order to obtain an insight about the metabolic state of mesquite in response to ZnO NPs, stress was quantified by the specific activity of the antioxidant enzymes CAT and APOX. Micro X-ray fluorescence (μXRF) technique has been successfully used to investigate the distribution and speciation of Zn in Arabidopsis plants.[6] In the present study, this technique was used to determine Zn speciation and distribution in mesquite plants treated with ZnO NPs. The objectives of this investigation were to evaluate the uptake and phytotoxicity of ZnO NPs on mesquite, the oxidation state and distribution of Zn in tissues and the effect of ZnO NPs on the activity of anti-ROS molecules. μXRF, X-ray absorption spectroscopy (XAS), and inductively coupled plasma-optical emission spectroscopy (ICP-OES) were used as analytical techniques.

2.2 Materials and methods

2.2.1 Preparation of ZnO suspensions.

The hexagonal ZnO NPs (10 nm) were purchased from Meliorum Technologies (Rochester, NY). Suspensions were prepared in a Hoagland modified nutrient solution previously described in the literature[7]. Zinc was present as a micronutrient in the Hoagland solution at a concentration of 0.37 μM. Dilutions were performed in order to obtain the desired ZnO NPs concentration (0, 500, 1000, 2000, and 4000 mg L−1) mixtures were stirred for 5 min and later sonicated for 30 min in an ice bath. All suspensions were freshly prepared before each experimental setup and adjusted to pH 5.8. To determine the NP aggregation, suspensions at concentrations varying from 500 to 4000 were prepared in the Hoagland modified nutrient solution. These suspensions were sonicated as previously described and pH adjusted to 5.8. After seven days under constant bubbling, the aggregation was determined using a light scattering VARIAN model PDDLS/Coolbatch 90T dynamic light scattering (DLS) with Precision Deconvolve 32 software (Bellingham, MA.)Paragraphs with the style *Heading 5,h5* applied can be extracted to appear in the table of contents as level 3 sub headings.

2.2.2 Seed Germination

Mesquite seeds were purchased from Granite Seeds (Lehi, UT). Seeds were presoaked for thirty minutes in 4% NaClO4 solution, rinsed 5 times with sterilized Millipore Water (MPW) and left overnight in sterilized MPW. Seeds were then placed in paper towels soaked with an antibiotic–antimycotic solution (A5955, Sigma, St. Louis, MO) to prevent fungal and bacterial contamination. After four days in the dark, plants were exposed to light for one more day and transferred to 200 mL jars containing a suspension of nanoparticles diluted in the nutrient solution. The seedlings were suspended in stock jars using polyurethane foam and plastic micropipettes on the top; therefore, only the roots were in contact with the nanoparticle suspension. Seedlings were allowed to grow for fifteen days at room temperature on a 16-h photoperiod (two 34 W Phillips lamps). During this period, the solution level was maintained

nearly constant by adding MPW every day. Triplicate sets of 40 plants/jar (200 mL) were set, for a total of 600 plants per experiment. Jars were continually aerated with aquarium pumps to provide oxygen and to maintain the NPs in suspension. Zinc ions were not included as treatments due to the very low solubility of the nanoparticles. For the zinc oxide the solubility was about 8 mg L−1 for the 4000 mg L^{-1} treatment.

2.2.3 Quantification of Zn in dry plant tissues.

For metal quantification, all plants were washed with 0.01 M HNO_3 and MPW to remove the NPs stuck on root surface. Subsequently, the plants were cut in roots, stems, and leaves and dried at 60 °C for 4 days. Next, samples were microwave digested using a CEM microwave (CEM Marsx, Mathews, NC). Samples treated with ZnO NPs were digested using 3 mL plasma pure HNO3 (SCP Science, New York) and diluted to 25 mL using MPW following the USEPA 3051 method (1200 W, 5 min ramping to 175 for 10 min at a pressure of 350PSI). Concentrations in plant parts were determined using ICP-OES. Certified standard reference materials (NIST-SRF 1570) of metals and metalloids (Metuchen, NJ) were used for calibration and quality assurance/quality control. In addition, an external certified standard of each element was used after every 10 samples to monitor the matrix effect on the analytes.

2.2.4 CAT/APOX assay

After 15 days of exposure to the NPs treatments, the plants were washed with 0.01 M HNO3 and MPW to remove any external contaminant. From every treatment, extracts of root, stem, and leaves of three plants were used to determine the activity of CAT according to Gallego et al.[7] with minor variations. For each treatment, a ratio of 10% (w/v) of root, stem or leaf samples was extracted with phosphate buffer (25 mM KH2PO4 at pH 7.4) by using a glass-glass homogenizer. Extracts were centrifuged for 5 min at 4 °C and 10,000 rpm in a refrigerated centrifuge (Eppendorf AG bench centrifuge 5417 R, Hamburg, Germany). Supernatants were transferred to microcentrifuge tubes for the assay[3]. A sample of 990 μL of 10 mM H2O2 was placed in a quartz cuvette and an aliquot of 10 μL of the sample was added to obtain a final

volume of 1 mL. The mixture was mixed by hand (shaken three times) and the absorbance at 240 nm was recorded in a Perkin Elmer Lambda 14 UV/Vis Spectrometer (single-beam mode, Perkin-Elmer, Uberlinger, Germany). The absorbance values were obtained from the first linear section of slope between 0.5 and 1 min. The extinction coefficient for H_2O_2 was set at 36.1 mM^{-1} cm^{-1}. The amount of protein for CAT/APOX was determined according to the Bradford method with serum albumin as standard[8].

APOX activity was evaluated according to Murguia et al. [9] with minor modifications. Extract of leaves were prepared as described above. The supernatant was separated after centrifugation. A volume of 886 μL of 0.1 M KH_2PO_4 buffer at pH 7.4, 10 μL of 17 mM H_2O_2, 100 μL of the sample, and 4 μL of a 25 mM solution of ascorbate were placed in a quartz cuvette and mixed. The absorbance was recorded at 265 nm in a Perkin Elmer Lambda 14 UV/Vis Spectrometer. The absorbance was recorded as described above and the extinction coefficient for H_2O_2 was experimentally set at 36.1 mM^{-1} cm^{-1}.

2.2.5 Micro XRF data acquisition

Roots of mesquite plants treated with 1000 mg ZnO NPs L^{-1} were washed twice with 0.01 M HNO3 and three times with DI water to eliminate any excess of NPs on the root surface. Roots were then sectioned in a Minotome plus cryostat (Triangle Biomedical Sciences, Durham, NC). Root samples were dissected 0.5 mm up from the root tip. Samples were frozen and embedded into specimen holders enclosed by Tissue Tek (Sakura Finetek USA, Inc., Torrance, CA). Samples were sectioned axially at 30 μm and 100 μm thick and mounted onto Kapton tape. Leaves were immersed in liquid nitrogen for 45 min and lyophilized at −53 °C and 0.140 mbar pressure for 3 days (Labcono FreeZone 4.5, Kansas City, MO). Micro-XRF mapping of the distribution of Zn and other elements in the leaves and roots was performed at beamline 10.3.2 of the Advanced Light Source, Lawrence Berkeley National Laboratory (ALS, Berkeley, CA) [10] Freeze-dried leaf and root sections were fixed on a x–y translation stage, cooled down to −20 °C to prevent radiation damage, and scanned under a micro focused beam. Maps were recorded

using a 5 μm × 5 μm beam and a 100-120 ms dwell time. The fluorescence yield was measured at an incident energy of 10 keV using a seven-element germanium (Ge) solid-state detector and normalized by I0 and the dwell time. Several bright and diffused points were selected from the XRF maps for Zn K-edge X-ray absorption near edge structure (XANES) analysis. XANES spectra were processed using a suite of programs available at beamline 10.3.2. Briefly, spectra were energy-calibrated with respect to a Zn foil (inflection point at 9658.76 eV) and the pre-edge background was subtracted and normalized using a linear pre-edge.

2.2.6 Statistics

The data reported for Zn uptake and CAT/APOX activity are averages of three replicates ± standard errors (SE). A one-way ANOVA test was performed followed by Tukey-HSD (honestly significant difference) test performed with the statistical package SPSS Version 12.0 (SPSS, Chicago, IL, USA). In all cases the statistical significance is based on a probability of $p < 0.05$.

2.2.7 XAS data acquisition

Plants from the 4000 mg ZnO L−1 treatment were cleaned with 4% NaClO solution, followed by rinsing with MPW. Roots, stems and leaves were immersed in liquid nitrogen for 45 min and lyophilized on a freeze dryer at −53 °C and 0.140 mbar pressure for 3 days (Labcono FreeZone 4.5, Kansas City, MO). After that, samples were homogenized in a mortar, loaded in aluminum sample holders, and covered with Kapton tape.

The XAS spectra were collected on beamline 7-3 at Stanford Synchrotron Radiation Light Source (SSRL, Palo Alto, CA). During data collection, the synchrotron radiation accelerator had a ring storage energy of 3 GeV and a beam current of 50–100 mA. Zn-K edge was collected using a Canberra 29-element germanium detector and Si(2 2 0) ψ 90 monochromator.

Zinc foil was used to calibrate sample spectra. Fluorescence and transmission mode were used for collecting all sample spectra and model compounds, respectively, at room temperature.

Zinc nitrate, and ZnO NPs were used as model compounds. The WinXAS software[11] was used to analyze the data. Edge energies from individual spectra were calibrated using the edge energy from the internal zinc foil (9659 eV). First and second degree derivatives of the inflection point of the metal foil were used to calibrate the sample spectrum, and a polynomial fitting subtraction was done in order to remove background. A first and fourth degree polynomial were used on the pre-edge and post edge region of the spectrum, respectively. Speciation of Zn was determined based on the XANES spectra from model compounds.[12]

2.3 Results and Discussion

2.3.1 CAT/APOX results Zn accumulation

The effects of ZnO NPs on CAT and APOX specific activity are shown in Figure 4. As seen in this figure, at all concentrations ZnO NPs increased CAT activity in roots (C1), stems (C2), and leaves (C3) (Figure 4). It seems that APOX activity changed in the whole plant by the mere presence of the ZnO NPs in roots. In addition, APOX response to ZnO NPs was different in each plant organ. As seen in Figure 4 1A1, the NP concentrations higher than 500 mg L−1 produced a reduction of APOX activity. However, APOX increased in the above ground plant parts at all ZnO NP concentrations, though in leaves the increase reached statistical significance only at 4000 mg L−1 (Figure 4, A1 and A2). A similar response was reported by Cuypers et al.[13] in common beans (Phaseolus vulgaris). These researchers reported that the mere contact of Zn with roots (50 μM) temporary reduced APOX activity in roots, but increased the activity of this enzyme in leaves. The plants were left in the NP suspensions for another 15 days (30 days in total), and even at the high NP concentrations, mesquite plants showed no visible signs of stress like chlorosis, necrosis, wilting or stunting.

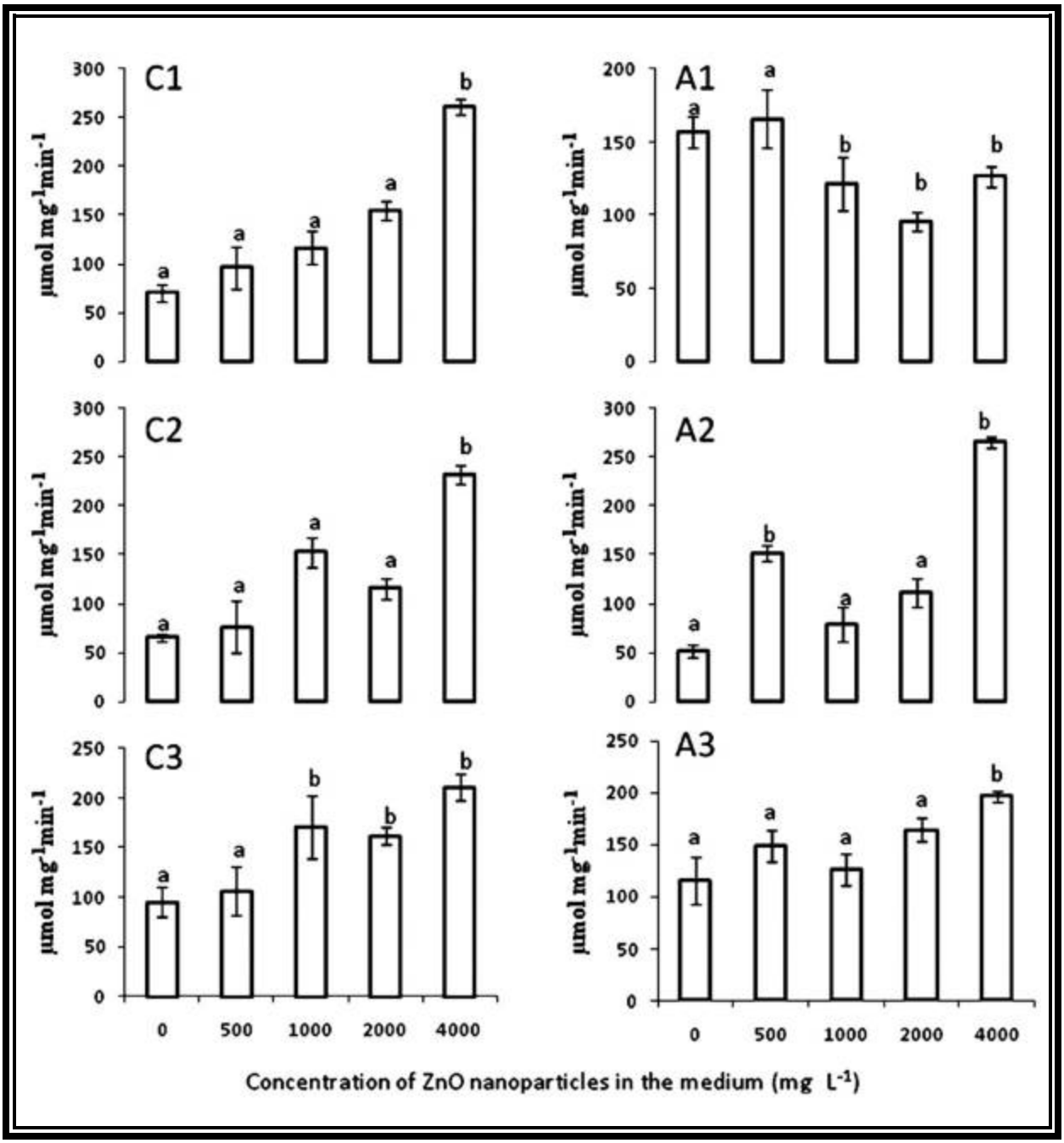

Figure 4: CAT (C) and APOX (A) specific activity in (1) roots, (2) stems, and (3) leaves of mesquite plants grown in hydroponics for 15 days under ZnO NPs treatment. Values are means ± SE. * Stands for significant differences at $p \leq 0.05$

2.3.2 Zn accumulation

The ICP-OES result from the certified reference material and external standards showed recoveries for zinc of 99%. Absorption of Zn by mesquite plants from the ZnO NP treatments is shown in Table 1. As seen in this table, at 500 mg ZnO NPs L^{-1} in the medium, the concentration of Zn in roots was about 3800 mg kg^{-1} d wt; however, in plants treated with 1000-4000 mg ZnO NPs L^{-1}, concentrations of Zn in roots varied from 2500 to 2000 mg Zn kg^{-1} d wt. These results could be determined by the aggregations of the NPs in the nutrient solution (Figure. 5). As seen in this figure, the average diameter of the particles at 500 mg L^{-1} (Figure 5B) was about 990 nm. Furthermore, at 500 mg L^{-1} there were particles with a diameter ≤100 nm resulting in more NPs and Zn ions available for plant uptake. Figure 5 also shows that at concentrations of 1000, 2000 and 4000 mg NPs L^{-1}, the NPs formed larger aggregates (Figure 5C-E), being the largest at 4000 mg L^{-1}. As previously reported[14], in aqueous environment NPs tend to attract each other and form aggregates. This process affects the mobility of NPs and can determine their final sink. Franklin et al.[15] reported that ZnO at 100 mg L^{-1} showed agglomeration resulting in flock formations of different sizes (nm to μm).

Table 1: Zinc concentration in roots, stems, and leaves of mesquite plants treated for 15 days in hydroponics with ZnO nanoparticles. Results are means ± SE. One-way ANOVA and Tukey's test were used to determine statistical significance. Means with same letter are statistically equals at $p \leq 0.05$.

(mg ZnO NPs L^{-1})	(mg Zn Kg^{-1} dry biomass)		
	Root	Stem	Leaf
Control	93±25a	59±2a	71±9a
500	3837±161b	1061±70b	423±77b
1000	2516±210b	949±33b	450±17b
2000	2102±87b	1135±56b	628±130b
4000	2017±122b	1113±96b	400±42b

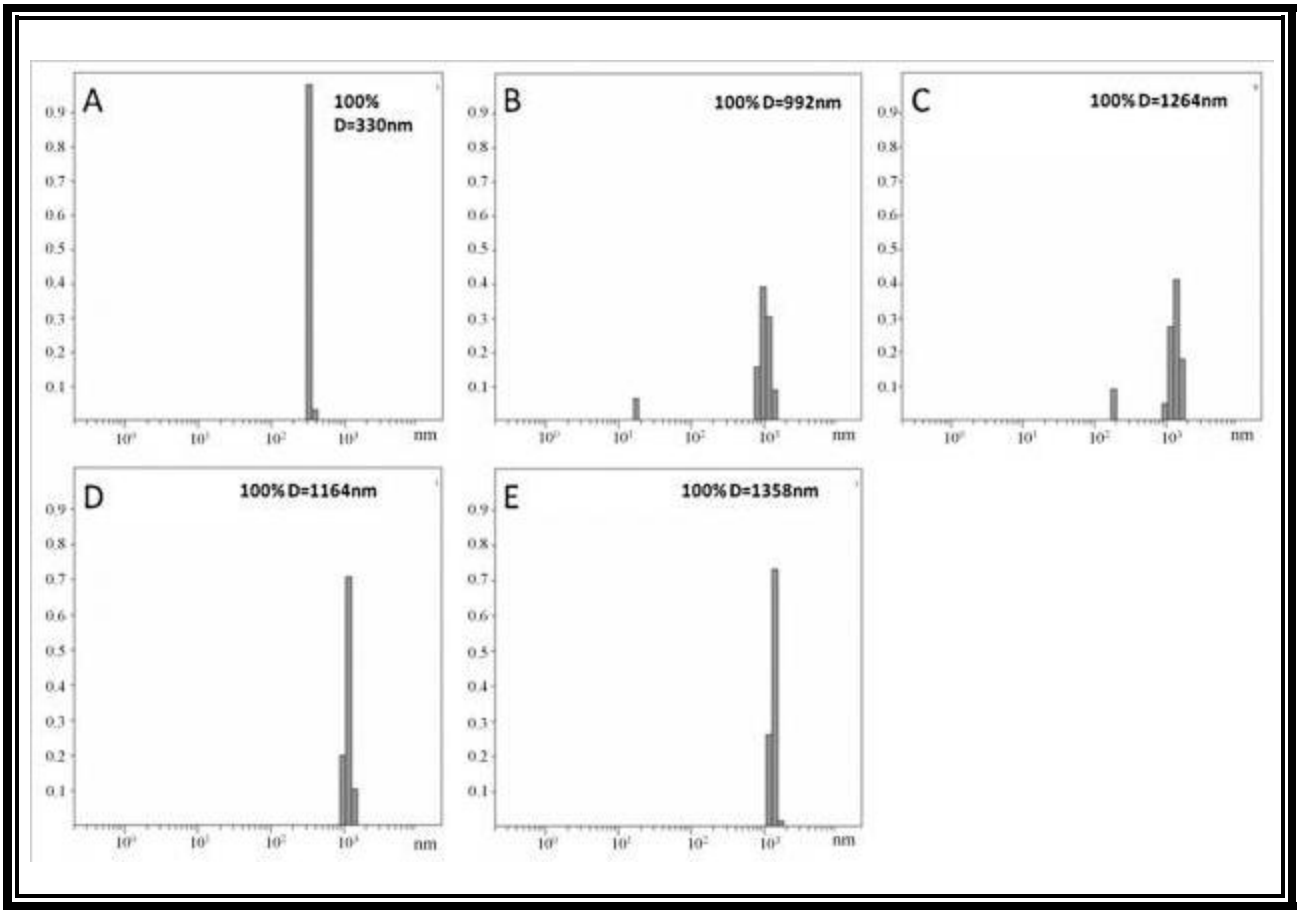

Figure 5: Dynamic light scattering determination of particle sizes in (A) nutrient solution, (B–E) nutrient solution with 500 mg L−1, 1000 mg L−1, 2000 mg L−1, and 4000 mg L−1, of ZnO NPs, respectively. The X axis shows particle diameter and the Y axis the normalized counts. The average particle diameter in nanometers is shown in the upper right corner.

Bioconcentration factors in roots (metal in roots/metal in medium) had indices of 7.6, 2.5, 1.0, and 0.5 for 500, 1000, 2000, and 4000 mg L^{-1} treatments. This reduction in the bioconcentration factors suggests that Zn in roots came from absorption, not from possible adsorption of the ZnO NPs on root surface. The data also suggest that mesquite plant did not transport much of the Zn concentrated in roots to the shoots. In all cases the translocation factors from roots to shoots were <1. It has been reported that Zn is required by more than 200 enzymes[16], and many of these enzymes are used by plants in roots to synthesize essential molecules[17]. Lin and Xing[18] reported that translocation factors of Zn from root to shoot in

Lolium perenne were very low under ZnO NP treatments, since the NPs were maintained in the apoplast and protoplast of the root endodermis and stele.

So far it is not possible to differentiate how much of the Zn in roots came from Zn dissociated from the NPs. However, de la Rosa et al.[19] have reported that the concentration of Zn ions in the supernatant of 500, 1000, 2000, and 4000 mg ZnO NPs L^{-1} solutions were 8, 32, 35, and 8 mg Zn L^{-1}, respectively, which suggests that most of the Zn in tissues came from the nanoparticles. More studies are needed to elucidate this issue.

2.3.3 XAS results

Figure 6 shows bulk XANES spectra of the model (pure) compounds (a) ZnO NPs and (b) $Zn(NO_3)_2$ as well as spectra of (c) leaves, (d) stems, and (e) roots of mesquite grown with ZnO NPs at 4000 mg L^{-1}. By comparing the XANES spectra obtained from mesquite plant tissues with spectra of the model compounds, it can be seen that in all mesquite tissues Zn was not present as ZnO NPs. The data could suggest that ZnO NPs were biotransformed on/in root surface and transported as Zn(II) from roots to leaves. This response differs slightly from the response found in mesquite treated with non-coated $Ni(OH)_2$ NPs. Non-coated $Ni(OH)_2$ NPs, were only partially biotransformed in roots but fully biotransformed in stems to a Ni-organic acid compounds.[20] In the present study, spectra showed that Zn was found as Zn(II) and resembled the spectra of $Zn(NO_3)_2$. This means that Zn was probably coordinated in the same manner as zinc nitrate (Figure 6). These results concurred with those obtained by Lopez-Moreno et al.[12] in soybean, where they found that within the tissues Zn was in the oxidation state of Zn(II) but not present as ZnO NPs. Further studies need to be done in order to clarify the possible uptake and biotransformation mechanisms of NPs in plants.

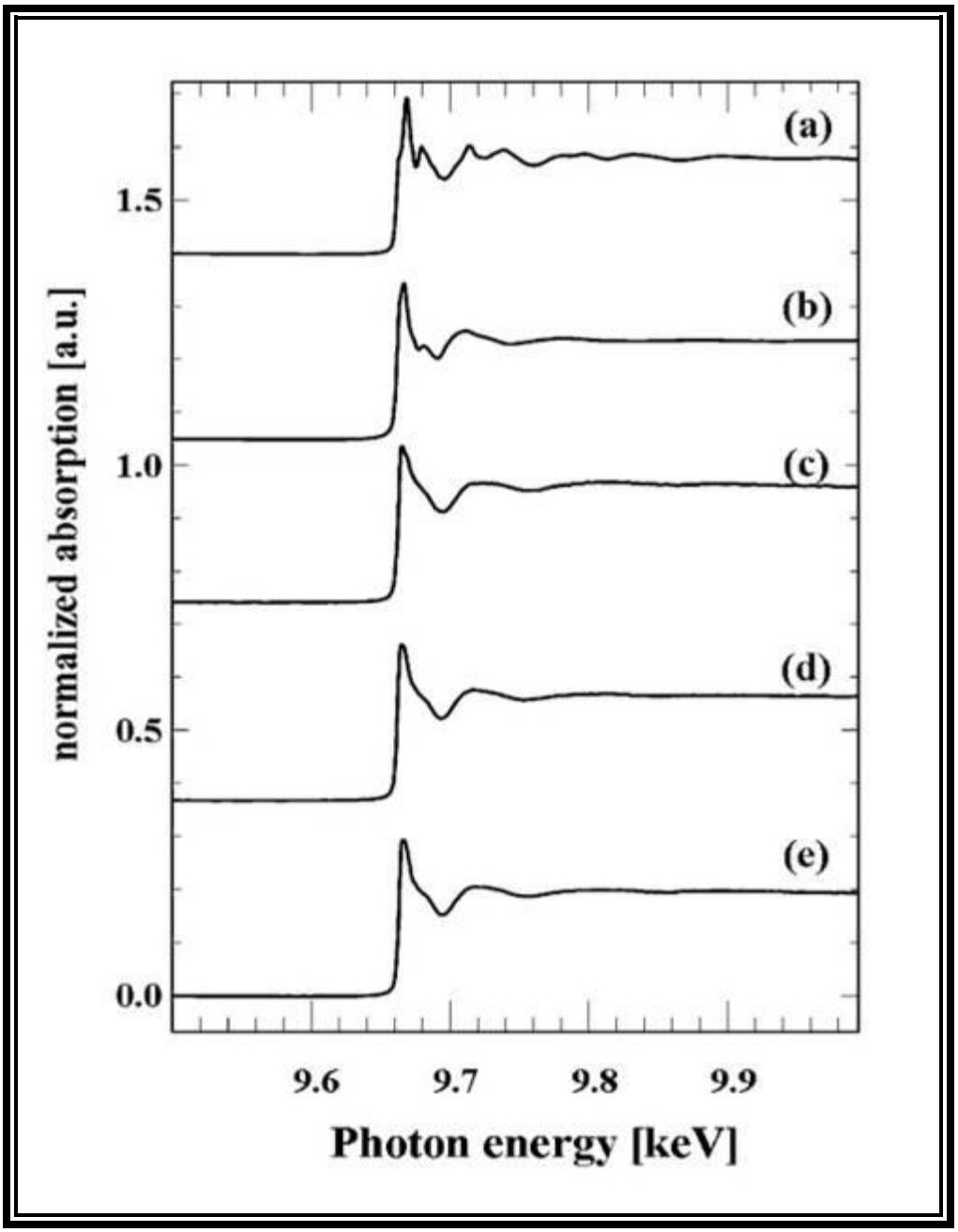

Figure 6: XANES K-edge spectra (9.659 keV) of the model compounds (a) ZnO NPs, and (b) $Zn(NO_3)_2$, and spectra of (c) leaves, (d) stems, and (e) roots of mesquite germinated in 4000 mg ZnO NPs L^{-1}.

2.3.4 XAS results μXFR results

Figure 7A shows a tricolour XRF map (potassium, zinc and calcium (K, Zn, Ca)) for control roots from plants grown in nanoparticle-free nutrient solution. The thickness of the control root was 100 μm in order to obtain higher Zn fluorescence signal and improve the quality of the map. Figure 7B and C shows the tricolour XRF maps of root samples treated with 1000 mg ZnO NPs L^{-1} (samples 30 μm thick). Although the thickness of NP treated samples was lower than the thickness of control samples, they showed a greater and brighter number of spots (Fig. 7B and C) compared to control (Figure 7A). This suggests that most of the Zn shown in Figure 7B and C was from the ZnO NPs. Figure 8 shows the XRF maps of the leaf control (Figure 8A) and leaf treated with 1000 mg ZnO NPs L^{-1} (Figure 8B). As shown in Figure 8B, leaves treated with ZnO NPs had more Zn in the vascular system compared to the control (Figure 8A). In the XRF maps, bright and diffuse fluorescence Zn spots were observed on several regions of the leaves and roots treated with ZnO NPs. K-edge μXANES was then performed on bright and diffuse spots of leaf and root μXRF maps. A total of 9 bright spots were selected: 3 marked from 0 to 2 in the root (Figure 7B) and 6, marked 0 to 5 in the leaf (Figure 8B). Pertaining to diffuse spots, a total of 11 spots were selected: 8 marked from 0 to 7 in root (Fig. 7C) and 3 marked from 6 to 8 in leaf (Figure 8B). Figure 9 compares the XANES spectra of ZnO NPs (pure compound) and the μXANES of the bright green spots and the diffuse spots from the root and leaf. The bright leaf and root spots spectra had almost identical spectral signature (Figure 9, lower spectra). These forms of Zn compounds are different from the forms obtained from the diffuse spectra. The diffuse root spots have a white line feature shifted to higher energy (9667 eV) and shorter period of the first oscillation above 9692 eV (Figure 9). Also, the amplitude of the first oscillation for both diffuse root and leaf spots was different indicating diverse Zn coordination environments. It is hypothesized that the shorter period in the spectra of the diffuse root possibly suggests an octahedral geometry. Different Zn ligands such as organic acids (malate, citrate and oxalate) and Zn phosphate have been identified by linear combination fittings to reference samples in the Zn accumulator plant Arabidopsis halleri[6]. However, there

were no clear findings from the XANES studies in mesquite. The organic acid content of the mesquite plants should be further studied in order to identify possible Zn organic ligands to use as references for XANES analysis.

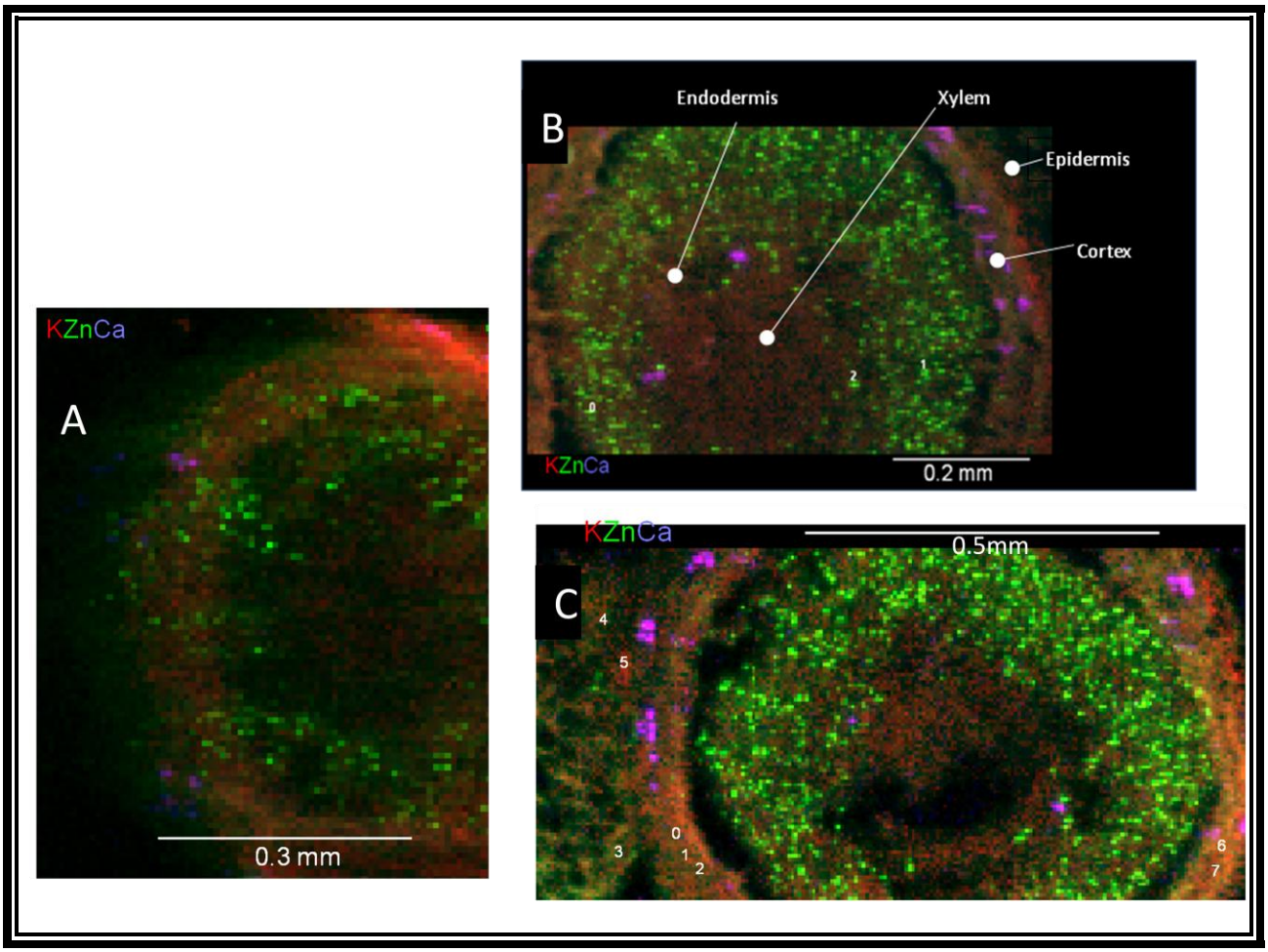

Figure 7: Tricolour micro-XRF images of the cross sections of (A) mesquite root control (sample of 100 µm of thickness); (B) and (C) two different mesquite roots samples treated with 1000 mg L−1 (sample of 30 µm of thickness). Red colour stands for potassium, green for zinc, and purple for calcium. In (B) and (C), bright spots are labelled with numbers from 0 to 2 and diffused spots with numbers 0 to 7.

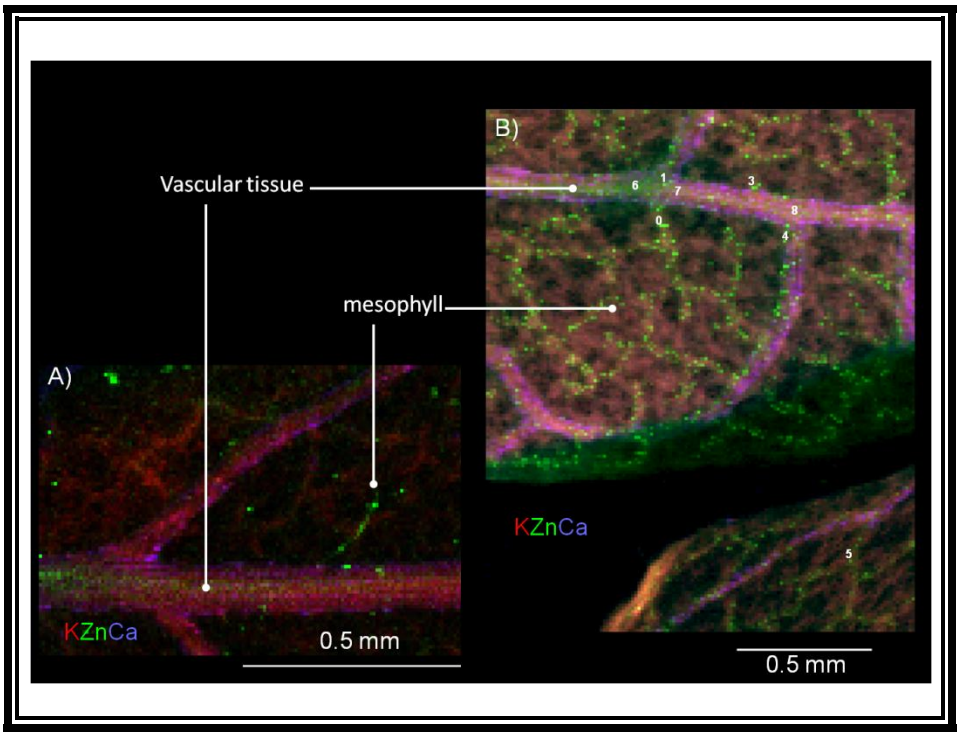

Figure 8: Tricolour micro-XRF images of (A) mesquite leaves control and (B) mesquite leaves treated with 1000 mg L−1. Red colour stands for potassium, green for zinc, and purple for calcium. In (B), bright spots are labelled with numbers from 0 to 5 and diffused spots with numbers 6 to 8.

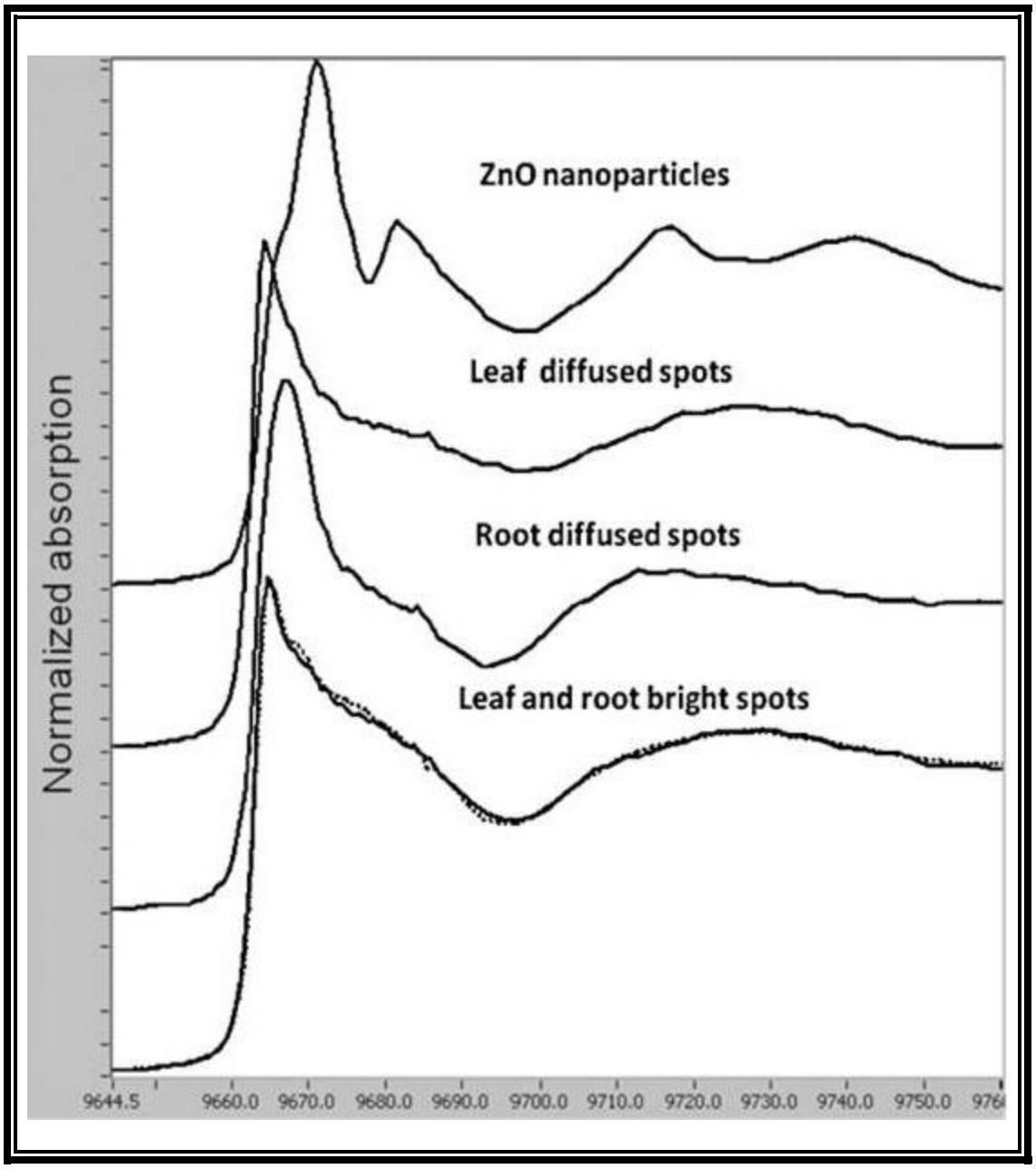

Figure 9: XANES region K-edge spectra of the ZnO NPs, and average spectra of the leaf and root diffuse and bright spots

2.4 Conclusion

The results of this study indicate that mesquite plants (P. juliflora-velutina) absorbed Zn from the NPs treatments as demonstrated by ICP OES. The reduction in the bioconcentration factors and the μXRF images suggest that Zn in roots came from absorption, not from possible adsorption of the ZnO NPs on root surface. Biochemical assays showed that the ZnO increased the specific activity of stress enzymes CAT in root, stem and leaves and APOX only in stem and leaves. However, mesquite plants showed no chlorosis, necrosis, stunting or wilting, even after 30 days of treatment, suggesting that this desert plant may display some tolerance to ZnO NPs and to the Zn ion released from these particles.

The XAS study showed no evidence of the presence of the ZnO NPs within tissues. Spectra show that Zn was found as Zn(II) and resembled the spectra of $Zn(NO_3)_2$. This means that Zn was probably coordinated in the same manner as zinc nitrate. The XANES analysis of the bright and diffused spots in μXRF maps of the root and leaf corroborated the biotransformation of the ZnO NPs and suggests the forms of Zn compounds in bright spots are different from the forms obtained from the diffuse spectra. This study demonstrated the importance of the use of μXRF and μXANES in the study of Zn accumulation by plants. The μXAS analyses are complementary to the bulk XAS studies as they allow observing changes in speciation with respect to localization.

CHAPTER 3

In Situ Synchrotron X‐ray Fluorescence Mapping and Speciation of CeO2 and ZnO Nanoparticles in Soil Cultivated Soybean (Glycine max)

Abstract

With the increased use of engineered nanomaterials such as ZnO and CeO2 nanoparticles (NPs), these materials will inevitably be released into the environment, with unknown consequences. In addition, the potential storage of these NPs or their biotransformed products in edible/reproductive organs of crop plants can cause them to enter into the food chain and the next plant generation. Few reports thus far have addressed the entire life cycle of plants grown in NP-contaminated soil. Soybean (Glycine max) seeds were germinated and grown to full maturity in organic farm soil amended with either ZnO NPs or CeO2 NPs. At harvest, synchrotron μ-XRF and μ-XANES analyses were performed on soybean tissues, including pods, to determine the forms of Ce and Zn in NP-treated plants. The X-ray absorption spectroscopy studies showed no presence of ZnO NPs within tissues. However, μ-XANES data showed O-bound Zn, in a form resembling Zn-citrate, which could be an important Zn complex in the soybean grains. On the other hand, the synchrotron μ-XANES results showed that Ce remained mostly as CeO_2 NPs within the plant. The data also showed that a small percentage of Ce(IV), the oxidation state of Ce in CeO_2 NPs, was biotransformed to Ce(III). Our results also showed that the plants exposed to CeO_2 diminished in growth but most importantly, nitrogen fixation was stopped at higher exposure concentrations. To our knowledge, this is the first report on the presence of CeO_2 and Zn compounds in the reproductive/edible portion of the soybean plant grown in farm soil with CeO_2 and ZnO NPs.

3.1 Introduction

Increasing production and use of nano-sized materials have raised concerns about their possible entry to the food supply with unknown consequences.[1] NPs can buildup on soil or plants through atmospheric routes such as the combustion process. Another route of exposure for agricultural crops is biosolids.[2,3] Amendments of soils with biosolids generated in wastewater treatment plants are a common practice worldwide. However, NPs are neither monitored nor regulated and have a high affinity for activated sludge bacteria, thus concentrating in biosolids. (e.g. biosolids accumulate up to 95% of CeO_2 NPs in wastewater treatment plants[4]). Furthermore, nano-sized fertilizers, pesticides and smart delivery nano-systems are currently being used or under development for agricultural use.[5]

Soybeans are the largest producers of edible oil and plant protein[6] and in 2010 were the fifth highest crop produced in the world and second in the USA.[7] This legume like many others is able to convert atmospheric nitrogen into nitrogenous compounds useful to the plant. This is due to a symbiotic relationship with root nodules that contain bacteria of the genus Rhizobium. Biotransformation of CeO_2 and ZnO NPs in hydroponically grown soybean seedlings has been studied with bulk X-ray absorption spectroscopy.[8] Synchrotron microfocused X-ray fluorescence (μ-XRF) and micro X-ray absorption near-edge structure (μ-XANES) have been used to determine the speciation of arsenic in the rhizosphere of mesquite (Prosopis juliflora-velutina)[9] and the relationship between speciation and distribution of zinc in the Zn hyperaccumulator Arabidopis halleri.[10] More recently, these techniques were used to study the chemical form and localization of titanium in cucumber (Cucumis sativus) plants treated with TiO_2 NPs[11] and the form of CeO_2 in roots of corn (Zea mays) seedlings.[12] To our knowledge this is the first study of plants grown to maturity in NPs impacted soil. The present report describes, with the use of μ-XRF and μ-XANES, the forms of Ce and Zn within soybean tissues, including the reproductive organ, and analyzes the possible transfer of nanoceria and ZnO NPs into the food chain. In addition, we studied the effects of NPs on the nodule nitrogen fixation potential.

3.2 Materials and methods

3.2.1 Soybean Growth

Organic farm soil (OFS) (from Carpinteria, CA, N 34° 23' 40'' , W 119°28 '40'') was sieved (2 mm), air-dried, and stored at 4 °C. The OFS was spiked with either ZnO (10 nm) or CeO_2 (8 nm) NPs (Meliorum Technologies, Rochester, NY) at concentrations of 0, 50, 100, and 500 $mg \cdot kg^{-1}$ for ZnO, and 0, 100, 500, and 1000 $mg \cdot kg^{-1}$ for CeO_2, 24 h prior to planting.

The characterization of these NPs was previously reported by Keller et al.[13] Dwarf soybean seeds (variety, Early Hakucho, product #5555) were acquired from Park Seed Company (Greenwood, SC). The planting methodology is described elsewhere.[14] Briefly, nodulating bacteria (Rhizobium japonicum

strain USDA 110) were added to the soybean seeds prior to the sowing. The seeds were planted in PVC trays for 4-7 days until cotyledons appeared. Later, the plantlets were transplanted to pots that contained 2400 g of soil. Four pots per treatment wereplanted, while another four were left unplanted as controls. A climate-controlled greenhouse under full sunlight with nominal maximum temperature of 27 °C was used for this experiment. Every 72 h, the pots were watered with 100 mL of tap water for days 1-9. The volume of water changed with plant growth: the pots received 200, 250, and 300 mL for days 9-21, 21-27, and 27-48, respectively. The unplanted pots received an average of 100 mL/day watering for the duration of the experiment. The plants were harvested after 48 days of growth.

3.2.2 Sample preparation for XAS analysis

At harvest, roots of soybean plants treated with 500 mg/kg of ZnO NPs and 1000 mg/kg of CeO_2 NPs were washed twice with 0.01 M HNO_3 and three times with deionized (DI) water to eliminate any surface contaminants.[14] Soybean plants were cut with a scalpel into root, nodule, low stem, high stem, and pod before transferring them to liquid nitrogen for 30 min. The plant parts were embedded in Tissue

Tek (Sakura Finetek USA, Torrance, CA) and axially sectioned (10 μm thick) with a cryomicrotome (Triangle Biomedical Sciences, Durham, NC) at -20 °C and mounted onto Kapton and Ultralene film. Sections were subsequently freeze-dried for 2 h in a Labconco freeze-dryer (FreeZone 4.5, Kansas City, MO) with operating conditions of -53 °C and 0.140 mBar pressure. For bulk XAS analysis, samples were flash frozen in liquid nitrogen and freeze-dried for 3 days. Afterward, dried tissues were ground to obtain a fine powder, loaded into aluminum sample holders, and covered with Kapton tape.

3.2.3 Nitrogen fixation Potential

To assess the effectsof NPs on nitrogenase enzyme activity of soybean root nodules, C_2O_2 reduction to C_2H_4 by nodules was measured, the methods are described elsewhere.[15,14] Briefly, Root nodules from treated soybean samples were washed and placed in sterile 60mL plastic syringes. The syringes were filled with 54mL of air followed by 6mL of C_2H_2. At 0, 15, 30, 45 and 60 minutes after C_2H_2 addition, 10 mL of gas from the syringe was injected to the gas chromatograph (SRI 8610; SRI instruments) equipped with a silica gel column. The parameters were as follow: Oven temperature of 145°C with carrier flow rate of 20 $mL*min^{-1}$. Two peaks were observed corresponding to C_2H_4 and C_2H_2. Peaks were turned into concentration by using standard curves, Calculations accounted for the decrease in total volume space over the course of sampling.

3.2.4 ICP OES and ICP MS analysis

Soil and tissue samples were analyzed for NPs metal content by ICP. Before ICP analysis, samples were digested by using a microwave acceleration reaction system (CEMCorp). Plant tissue samples treated with nano-ZnO were digested by using Environmental Protection Agency method 3051. Soil samples were digested with a mixture of concentrated plasma-pureHNO3 and HCl (1:3; i.e., aqua regia). The nano-CeO2 treated samples were digested with concentrated plasma-pure HNO3 and H2O2 [30% (vol/vol); 1:4] as described previously[16] with slight modifications. Ten blanks were analyzed to calculate the detection limit for Zn and Ce.

Standard reference materials from National Institute of Standards and Technology 1547, 1570a, and 2709a were used to validate the digestion and analytical method obtaining recoveries between 90% and 99%. For quality control of the ICP readings, every 10 samples, the blank and a spiked sample containing Ce and Zn at 10 mg·L−1 were read. The average readings for Ce and Zn in the spiked samples were 10.1 ± 0.30 mg·L−1 and 9.9 ± 0.20, respectively. The total Ce and Zn concentrations in the tissues and soil were determined using ICP-OES (Optima 4300 DV; Perkin-Elmer) and ICP-MS (ELAN DRC II; Perkin-Elmer). Zn-treated samples were analyzed with ICP-OES, whereas Ce-treated and control samples were analyzed with ICP-OES and ICP-MS. ICPMS allowed for the detection of trace amounts of Ce in the plant tissue. The ICP-OES parameters used were as follows: nebulizer flow, 0.80 $L \cdot min^{-1}$; power, 1,450 W; peristaltic pump rate, 1.5 $mL \cdot min^{-1}$; flush time, 15 s; delay time, 20 s; read time, 10 s; and wash time, 60 s. Every sample was read in triplicate. The ICP-MS parameters used were as follows: plasma radiofrequency power, 1,400 W; plasma gas flow (Ar), 18 l min^{-1}; scanning mode peak hopping; nebulizer flow, 0.95 l min^{-1}; dwell time, 35 ms; sweeps, 30; and replicates, 3.

3.2.5 μ-XRF and μ-XANES Studies at ESRF

μ-XRF mapping of the distribution of Ce and other elements in the soybean plant was performed with an incident energy of 5.8 KeV during 16-bunch mode at beamline ID21 of the European Synchrotron Radiation Facility (ESRF, Grenoble, France).40 The storage ring current during data acquisition ranged between 60 and 90 mA operating at 6.0 GeV. The beam was focused with the use of K-B optics to 0.60 x 1.1 μm2 (V x H). The fluorescence signal was detected by a Si drift detector. Two photodiodes were used to measure the incident and transmitted beam intensities. Dwell time and distance of the detector were optimized for each image, keeping the detector dead time below 15%. The X-ray fluorescence data were processed using PyMCA software.[17] For μ-XANES data acquisition, the energy was selected using a Si(111) monochromator and scanned from 5.70 to 5.80 keV. The final Ce L(III) edge spectra were the sum of 5-60 individual scans with 0.1 s integration time and 0.5 eV step size. Each

individual spectrum was inspected for beam induced changes, and the samples were stable in all cases. μ-XANES data analysis was carried out using Athena software.[18] The linear combinations fit range was 5.700-5.780 and 9.600-9.800 keV for Ce and Zn samples, respectively. Normalized sum of square residuals were used as a measure of the discrepancy between the unknown data and the fit model.

For the PF data analysis, the pre-edge background was subtracted and normalized using a linear pre-edge. All peaks were identified by least-squares fitting of Gaussian profiles and one arctangent function.[19]

2.2.6 μ-XRF and μ-XANES Studies at SSRL

Synchrotron experiments were conducted at SSRL beamline 2-3, which uses K-B optics to achieve an optimized beam with dimensions of 2 x 2 μm. μ-XRF mapping was performed with 0.5 x0.5 μm2 step size and 250 ms dwell time using a Si(111) monochromator for energy selection and Vortex (SII) detector for X-ray fluorescence detection. μ-XRF images and μ-XANES data were analyzed using the Micro Analysis Toolkit44 and SixPACK.[20] The Zn foil calibration was set at 9.659 keV. The data processing included dead time correction, multiple sweep data inspection to deglitch individual scans, energy calibration, spectral averaging, background subtraction, principal component analysis, and linear combination fitting to reference spectra. Beamline 6-2 was used to collect transmission X-ray microscopy (TXM) images above the Zn K-edge (9.7 keV) with optics providing 30 nm resolution and 30 μm field of view. Multiple fields of view were acquired by raster scanning the sample. XANES were collected using aVortex (SII) detector in fluorescence mode, with slits narrowed to create a 5 μm beam size. Beamline 7-3 was used to analyze the model compounds and bulk soybean samples exposed to ZnO NPs. The operating conditions in the storage ring were 3 GeV beam energy, an 80-100 mA beam current. Zn K-edge spectra were collected using a Canberra 29-element germanium detector and Si(220) ψ90 monochromator.

3.3 Results and Discussion

ICP-OES and ICP-MS data showed that soybean plants grown in organic farm soil spiked with ZnO or CeO2 NPs take up and translocate Zn and Ce throughout the plant (Table 2). Based on the concentration of the analytes, the μ-XRF and μ-XANES analyses were focused on the nodules since these are part of the root system and involved in the nitrogen fixation process. In addition, we focused our spectroscopic studies on the soybean pod due to its importance in the food industry. Figure 10A shows the Ce L(III) XANES spectra of Ce model compounds Ce acetate, Ce carbonate, CeO2 NPs, Ce sulfate, and Ce hydroxide. We used these as reference compounds in order to perform linear combination fitting (LCF) analysis of the plant samples to determine speciation of Ce. Figure 11a shows an optical micrograph of the transverse section of a root nodule from a soybean plant grown in soil with CeO_2 NPs, while Figure 11b shows the μ-XRF Ce intensity map of the nodule. As shown in Figure 11b, Ce was mainly localized in the epidermis; however, Ce was also observed inside the nodule. Figure 11c shows the spectra from the high intensity Ce spots and the LCF. From the LCF, it was estimated that

Table 2: Concentration, mg·kg−1 dry tissue. †,‡*No significant difference within plant part among treatments, i.e., P > 0.05 (t test) vs. other entries in the same column with a matching symbol.ψ Multiplied by 1,000; units are μg Ce·kg−1 dry tissue.

		Root	Nodule	Stem	Leaf	Pod
	Control	31.61 ± 2.12	19.68 ± 3.59*	19.48 ± 1.46	85.59 ± 7.59	32.04 ± 2.83*
ZnO	50	46.14 ± 1.44*	9.21 ± 8.03*	32.94 ± 3.58	125.76 ± 10.14	38.69 ± 3.13*
	100	45.73 ± 4.10*	24.20 ± 3.61*†	46.63 ± 4.27	165.98 ± 15.41	57.46 ± 5.75
	500	123.16 ± 11.67	34.77 ± 3.94†	126.23 ± 8.91	344.07 ± 43.12	81.69 ± 3.19
CeO_2	Control	0.296 ± 0.02	0.117 ± 0.02	0.039 ± 0.00†	0.177 ± 0.02†ψ	0.074 ± 0.03†
	100	0.490 ± 0.07	0.427 ± 0.02	0.169 ± 0.05‡	0.112 ± 0.01ψ	0.101 ± 0.02†
	500	174.46 ± 28.25†	19.83 ± 5.42†	0.206 ± 0.10†,‡	0.247 ± 0.03†,‡ψ	0.133 ± 0.07
	1000	210.72 ± 17.21†	11.28 ± 5.01†	0.116 ± 0.04†,‡	0.289 ± 0.04‡ψ	0.090 ± 0.03†

approximately 79% of the Ce was bound as CeO_2, maintaining the original CeO_2 NP coordination. This corroborates the scanning transmission electron microscopy and energy-

dispersive spectroscopy (STEM EDS) results that showed particulate accumulations of Ce in the soybean nodules.[14] The tricolor μ-XRF map of the soybean pods (Figure 12a) shows low intensity Ce signal spots, which demonstrates that low amounts of Ce were translocated to the pod. This agrees with the concentrations obtained from the ICP-OES and ICP-MS results (Table 2). μ-XANES spectra were also acquired from a few selected spots within the area scanned in the μ-XRF Ce intensity map and tricolor map (Figure 12b,c, respectively). Figure 12d shows that the analyzed spectra from the μ-XRF Ce intensity map resemble the CeO_2 NPs spectra, and the LCF data corroborate that 88% of the Ce in the analyzed spots were associated in the same way as the CeO_2 NP model compound. This suggests that most of the Ce was stored in the soybean pods as CeO_2 NPs. Previous bulk XANES analyses on alfalfa (Medicago sativa), corn, cucumber, and tomato (Solanum lycopersicum) seedling samples treated with CeO2 NPs in hydroponics showed that CeO_2 NPs were the main chemical species of Ce within the plantlets.[21] Furthermore, Zhao et al.,[11] using μ-XRF and μ-XANES techniques, found that Ce was coordinated as CeO_2 NPs inside the roots of corn plants grown in organic soil amended with alginic acid coated CeO_2 NPs. Zhao et al.[11] also reported confocal microscopy images of fluorescein isothiocyanate-stained CeO_2 NPs in the cell walls of corn root cortex, suggesting passive uptake of the CeO_2 NPs.

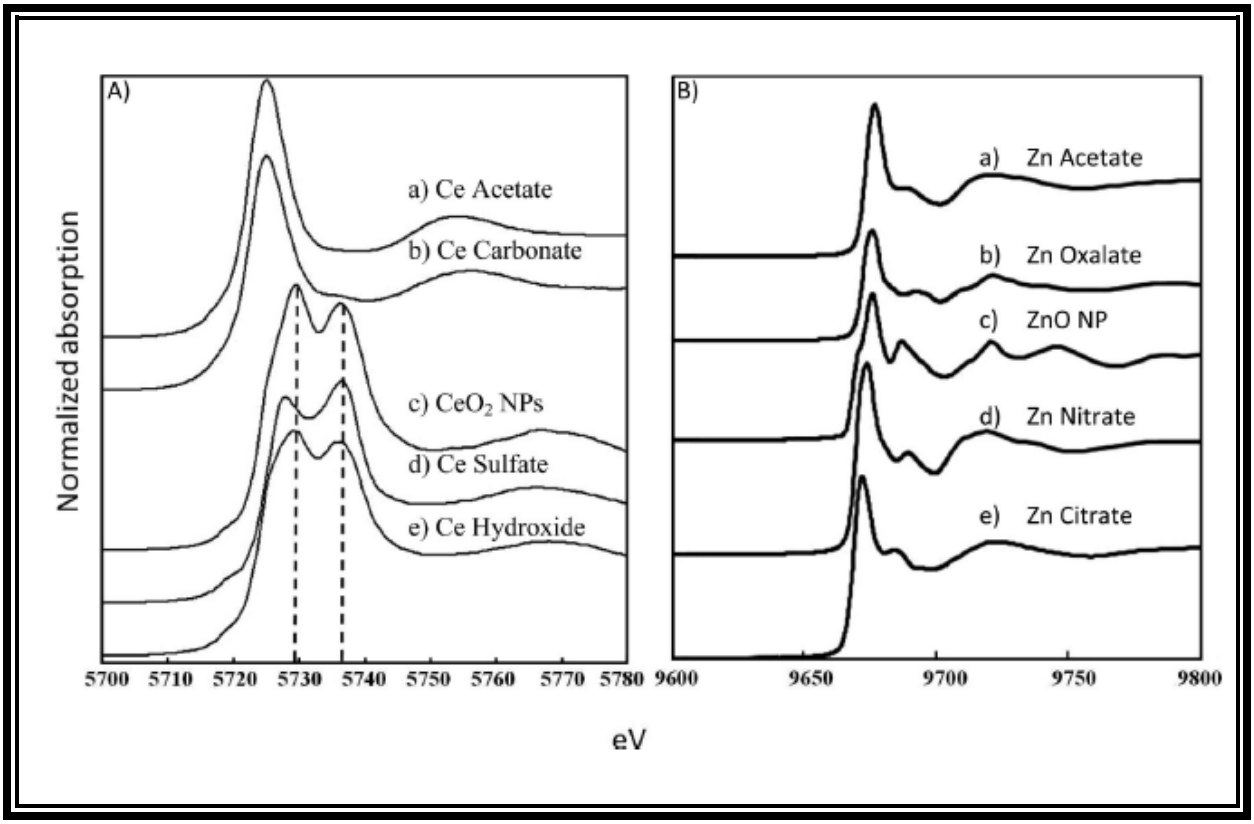

Figure 10: (A) Ce L(III) XANES of the Ce model compounds. Dotted lines at 5729 and 5737 eV illustrate the characteristic double white line in Ce(IV). (B) Zn K-edge XANES of the Zn model compounds.

In order to obtain further insights into the speciation of Ce in soybean plants, a peak fitting (PF) data analysis method was performed on the soybean pod and nodule high intensity Ce spots. The double white line marks at 5729 and 5737 eV present in the spectra from all of the analyzed spots (pod and nodule) show a signature, where Ce is mainly present in the Ce(IV) oxidation state (e.g., compounds in Figure 10A). However, compared with the CeO2 NP spectra (Figure 13b), the spectra from the Ce high intensity spots in the soybean pod show an increase in the amplitude (area) of peak C (Figure 13a). This can be attributed to an increased contribution of Ce(III) in the sample. The results suggest that internalization of CeO_2 within the soybean pod is affecting the structural order of Ce, which in turn can provide a surface susceptible for reduction. Similarly, Zhao et al. found that the interaction of CeO_2 NPs with corn plant roots affected the oxidation state of Ce.[11] In the present work, a reduction in the intensity of the white

line feature, compared with the CeO2 NPs, was observed (Figure 13). Roggenbuck et al. reported a similar result in a comparison study of nanoporous CeO2 and bulk CeO2, attributed to a change in the surface-to-volume ratio.[12] Figure 10B shows the XANES spectra of the Zn model compounds used for LCF. These model compounds included ZnO NPs, Zn-acetate, Zn-citrate, Zn-nitrate, and Zn-oxalate. These spectra were used to compare with spectra from ZnO NP-treated samples.

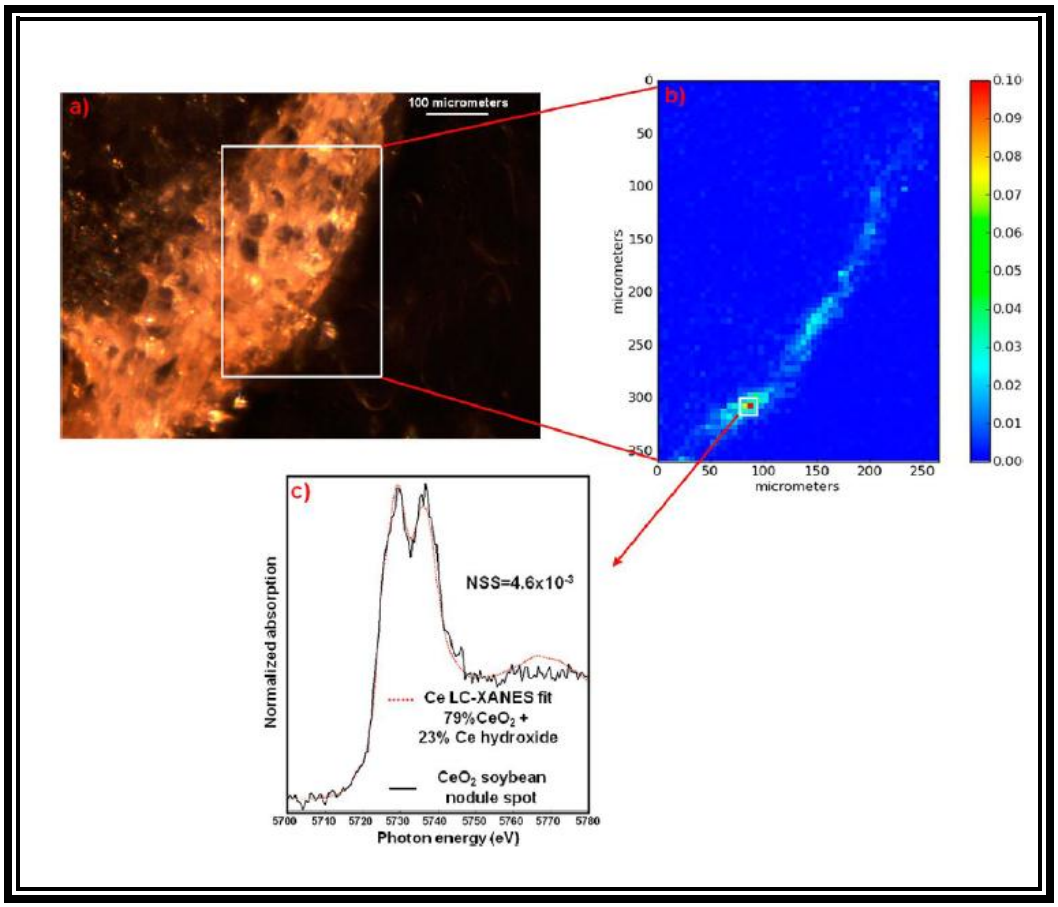

Figure 11: Images of the transversal section of a nodule from soybean plant grown in soil treated with 1000 mg of CeO2/kg. (a) Video microscope image of the nodule section. (b) μ-XRF temperature map showing normalized Ce intensity; red represents higher Ce intensity, and dark blue represents the absence of a Ce signal. The white box area indicates where μ-XANES was acquired. (c) Ce L(III) μ-XANES from a high intensity Ce spot in the nodule (solid, black color) and the spectra from the linear combination fitting (dotted, red color). Normalized sum-squared residuals (NSS) are shown next to the fitting. NSS = $\Sigma 1(\text{XANESexperimental} - \text{XANESfit})^2/\Sigma 1(\text{XANESexperimental})$.

Figure 14 shows tricolor maps obtained from the μ-XRF images of the nodule, stem, and pod. The concentration for Zn (Table 2) in both the control and treated samples indicates that the soybean plants translocate Zn to the aerial portion of the plant. The highest concentration of Zn in the nodule was in the epidermis, where high Zn intensity spots can be observed (Figure 14a). The μ-XRF image from the soybean stem (Figure 14b) shows that most of the Zn was found in the phloem, which is part of the vascular system of the plant. Riesen and Feller[22] reported that, compared to other heavy metals, radiolabeled Zn was preferentially accumulated in the phloem of wheat plants (TriticumaestivumL. cv. "Arina"). As can be observed in the μ-XRF map (Figure 14c), we found high Zn intensity signals in the outer pod, although Zn was also present in the soybean grain. White marks in Figure 14 represent areas with high Zn intensity in the μ-XRF map. These areas were chosen in order to perform μ-XANES analysis. The results from all of the analyzed spectra (Figure 15) suggest that the Zn within the soybean plant was no longer in the form of ZnO NPs. We also performed synchrotron-based TXM studies on the soybean pod (Figure 16). From the Zn micro-XRF intensity map (Figure 16a), a high intensity section was chosen to perform TXM at 30 nm resolution. Dark precipitates are observed in Figure 16b,c; these dark structures were confirmed to be Zn by the μ-XANES Zn-edge signal (Figure 15d). The spectra from the Zn precipitate (Figure 15d) did not correctly fit any of our model compounds; however, they share a high level of resemblance with the Zn-citrate spectra (Figure 15e), indicating Zn-O ligation. Other researchers have suggested the possibility of Zn precipitation on cowpea root (Vigna unguiculata).[23] On the other hand, Figure 15 shows spectra taken from the μ-XRF tricolor maps (Figure 14, white squares). The spectra from the nodule (Figure 15c) had closest similarity to the Zn-citrate and Zn-nitrate, whereas the stem and pod spectra show a closest fit to Zn-citrate (Figure 15a,b). However, we are well aware that the accuracy of the LCF rests on the model compounds. Sarret and co-workers found that spectra of a mixture of organic acids (malate, citrate, and oxalate) and Znphosphate had a close fit with spectra from the hyperaccumulator plant Arabidopsis halleri.[10] We have observed similar results in previous studies of mesquite (Prosopis juliflora-velutina) exposed to ZnO NPs, where the μ-

XANES spectra suggested a Zn-O ligand. However, the study from Thangavel et al.[24] on cell suspension cultures of red spruce (Picea rubens Sarg.) suggests that, in living cells, it is likely that Zn ions bind to

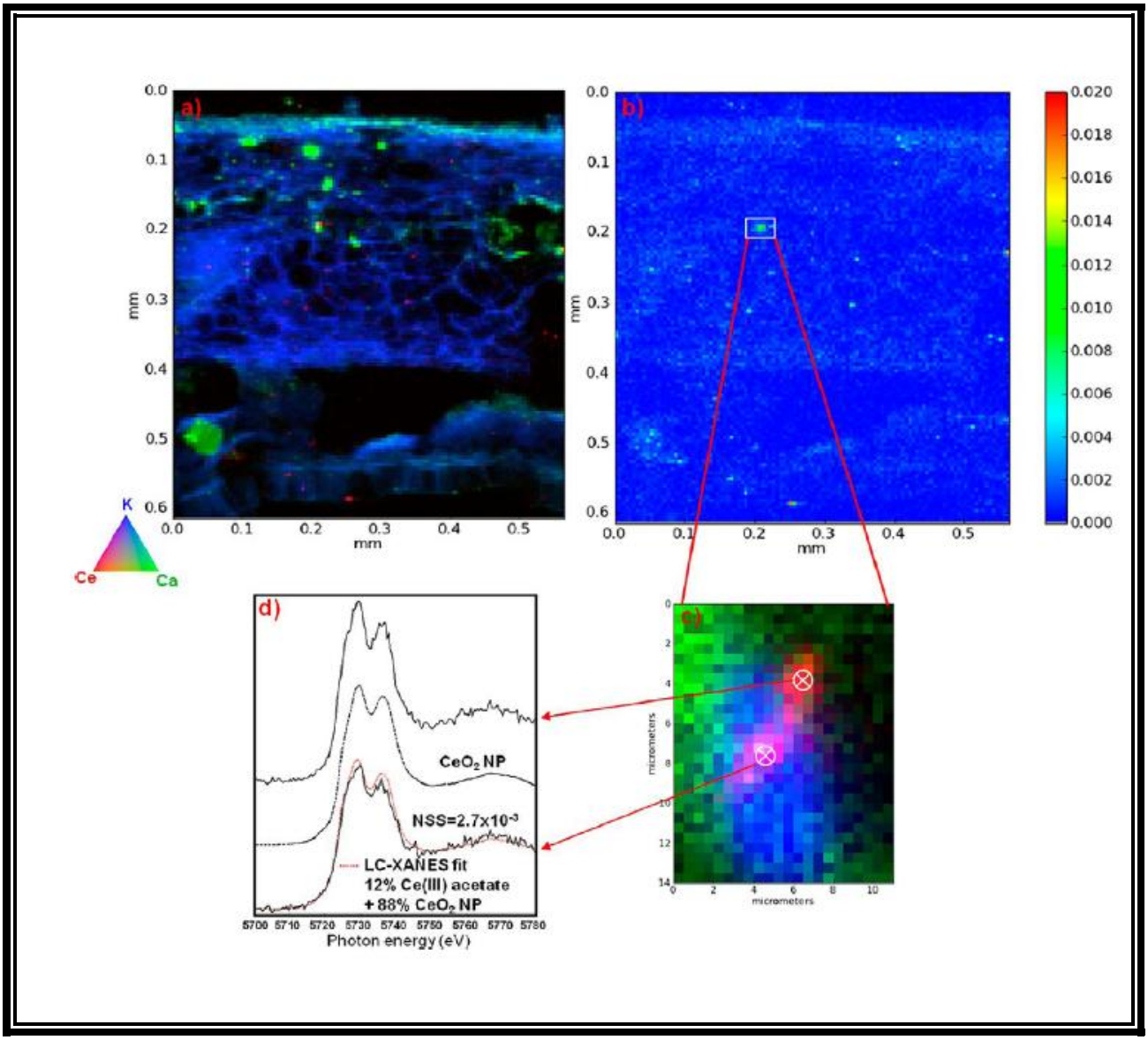

Figure 12: Images of the transversal section of a soybean pod grown in soil treated with 1000mgof CeO2/kg. (a) Tricolor µ-XRF map (red = Ce, green = Ca, blue = K). (b) µ-XRF temperature map of same location in (a) showing normalized Ce intensity. (c) Blowup of tricolor µ-XRF map from (b) (red = Ce, green = Ca, blue = K). White cross marks indicate where Ce L(III) µ-XANES were collected. (d) Ce L(III) µ-XANES spectra from selected spots, CeO2 NP model compound, and the spectra from the linear combination fitting (dotted, red color). Normalized sum-squared residuals (NSS) are shown next to the fitting. NSS = Σ1(XANESexperimental - XANESfit)2/Σ1(XANESexperimental).

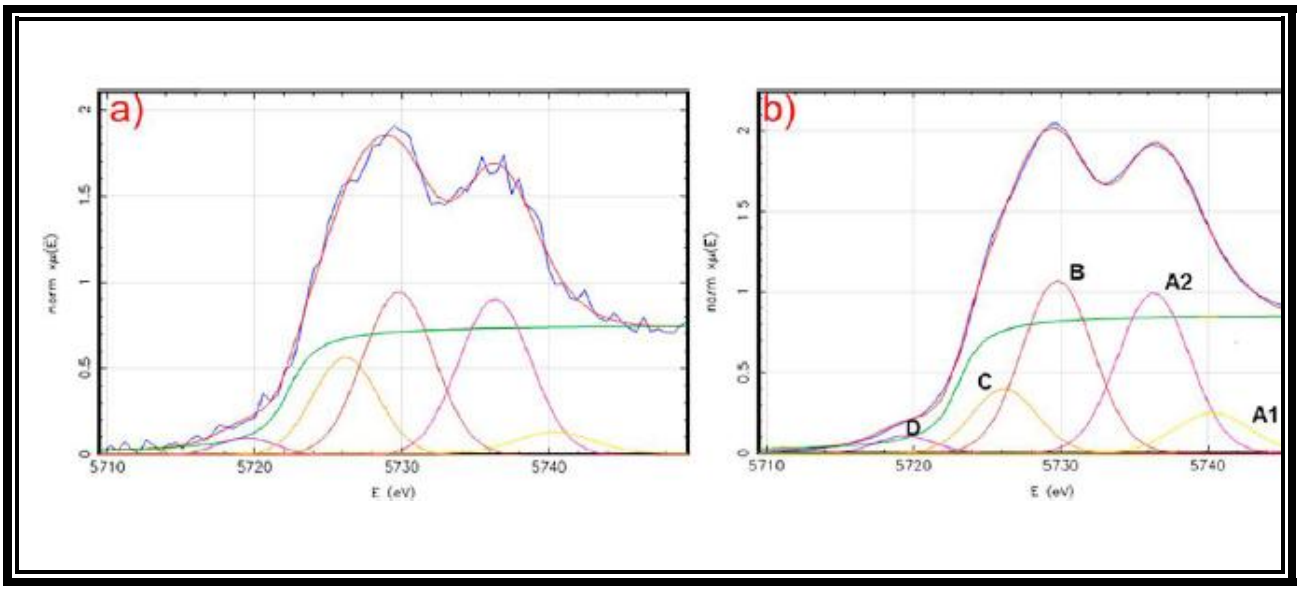

Figure 13: Images of the transversal section of a soybean pod grown in soil treated with 1000mgof CeO2/kg. (a) Tricolor μ-XRF map (red = Ce, green = Ca, blue = K). (b) μ-XRF temperature map of same location in (a) showing normalized Ce intensity. (c) Blowup of tricolor μ-XRF map from (b) (red = Ce, green = Ca, blue = K). White cross marks indicate where Ce L(III) μ-XANES were collected. (d) Ce L(III) μ-XANES spectra from selected spots, CeO2 NP model compound, and the spectra from the linear combination fitting (dotted, red color). Normalized sum-squared residuals (NSS) are shown next to the fitting. NSS = Σ1(XANESexperimental - XANESfit)2/Σ1(XANESexperimental).

the sulfur of phytochelatins rather than to oxygen of organic acids. The ZnO NPs or their dissociated Zn ions could trigger the biosynthesis of phytochelatins, which are well-known indicators of heavy metal toxicity in plants. Nevertheless, all of the μ-XANES and linear combination data from high Zn intensity spots in the μ-XRF maps suggest that Zn(II) in the soybean plants was associated with oxygen because its spectra resemble the spectra of organic acids from the model compounds (Figure 15). LCF of bulk XANES of ground up plant tissues also indicated Zn ligation to O (data not shown). Lombi et al.[25] used a novel detector for complex natural samples (Maia detection system) to minimize radiation damage and dehydration of samples. By using the same detector, Kopittke and co-workers analyzed cowpea (Vigna unguiculata) exposed to Zn.[23] These investigators also found a ZnO bond and determined that 65-85% of the Zn was bound as a Zn-phytate complex. Phytic acid is present in soybean plants

and is the main form of phosphorus storage.[26] However, for this investigation, we did not have a Zn-phytate model compound. Nevertheless, by comparing the spectral shapes from Zn-phytate with the Zn in the soybean, we concluded they were not a good match. Table 3 shows the N_2 fixation potential of nodules exposed to the metal oxides NPs. The fixation potential was similar between the nodules exposed to ZnO NPs. On the other hand, nodules exposed to 500 and 1000 $mg*Kg^{-1}$ of CeO_2 decreased its N_2 fixation potential by more than 80% relative to the control. This effect has previously been reported with cadmium exposure.[27]

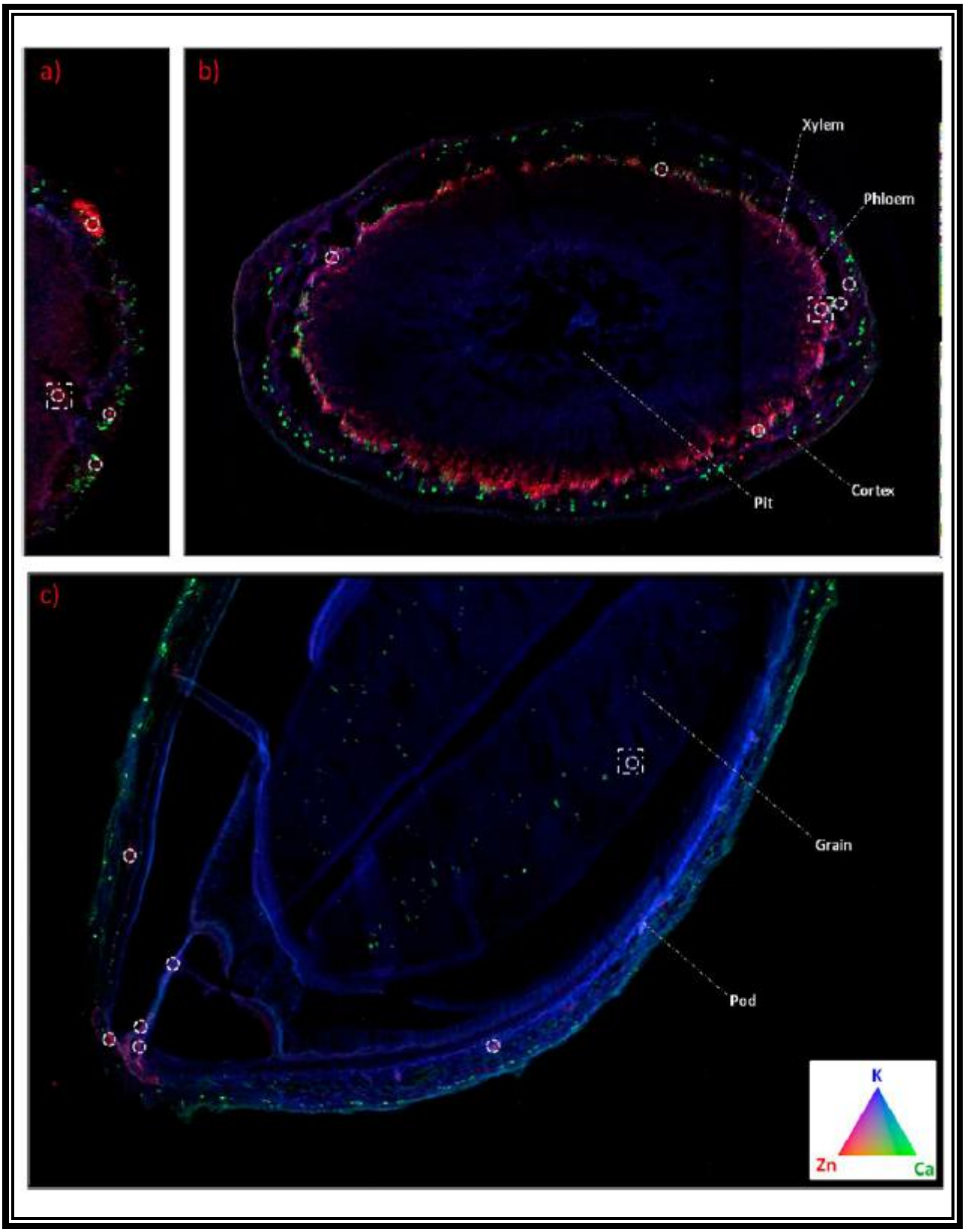

Figure 14. Tricolor μ-XRF maps (red = Zn, green = Ca, blue = K): (a) nodule, (b) stem, and (c) pod maps. μ-XANES was performedin areas of high Zn intensity marked by white circles. White square denotes the area from which spectra are shown in Figure 15.

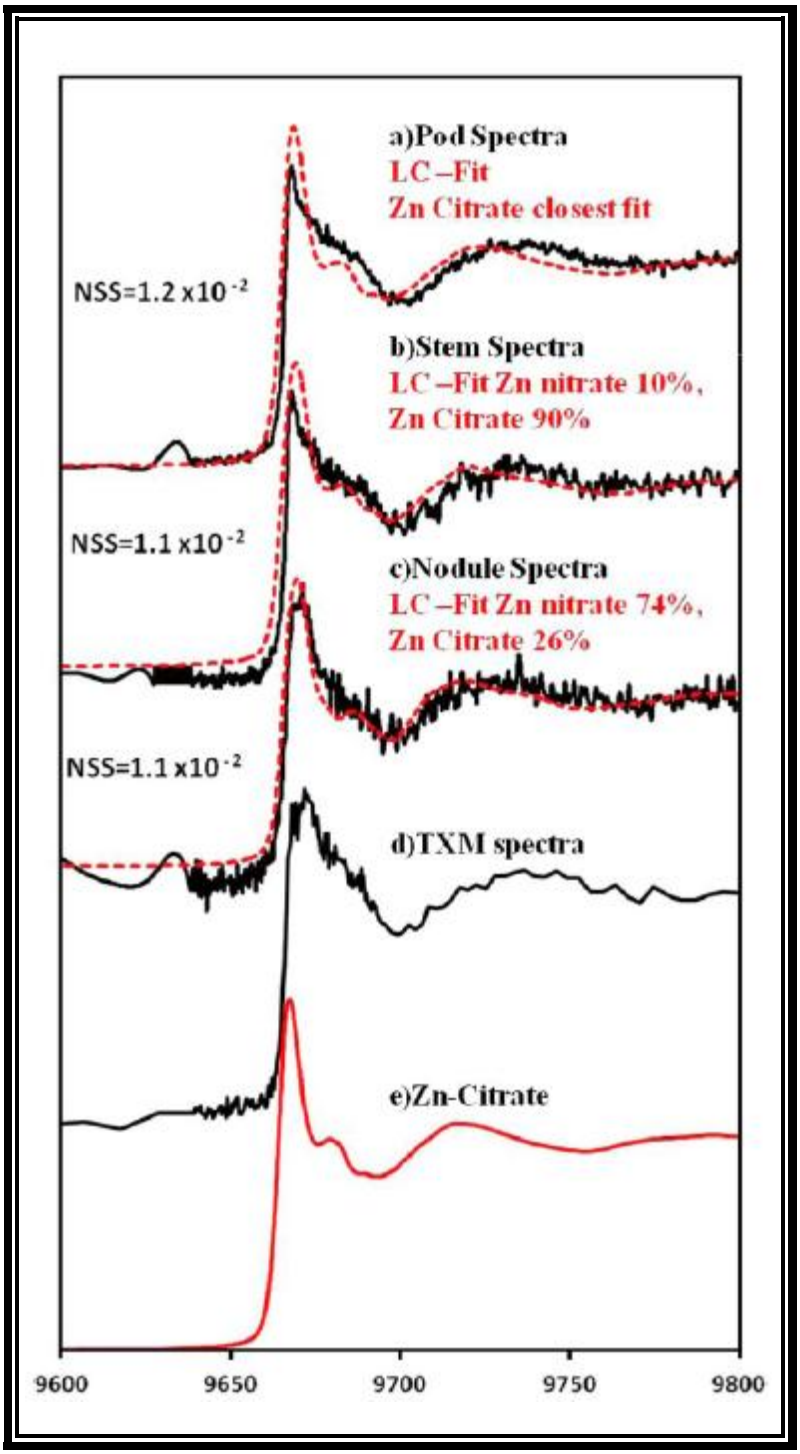

Figure 15. Zn K-edge XANES spectra from soybean samples grown with ZnO NPs in the soil. Linear combination fittings for (a) pod, (b) stem, and (c) nodule. Spectra with red dotted lines represent fits, and black solid line spectra represent μ-XANES from the sample. Normalized sum-squared residuals (NSS) are shown next to the fitting. (d) TXM spectra from the area indicated in (b. (e) Zn citratemodel compound.Figure 14. Tricolor μ-XRF maps (red = Zn, green = Ca, blue = K): (a) nodule, (b) stem, and (c) pod maps.

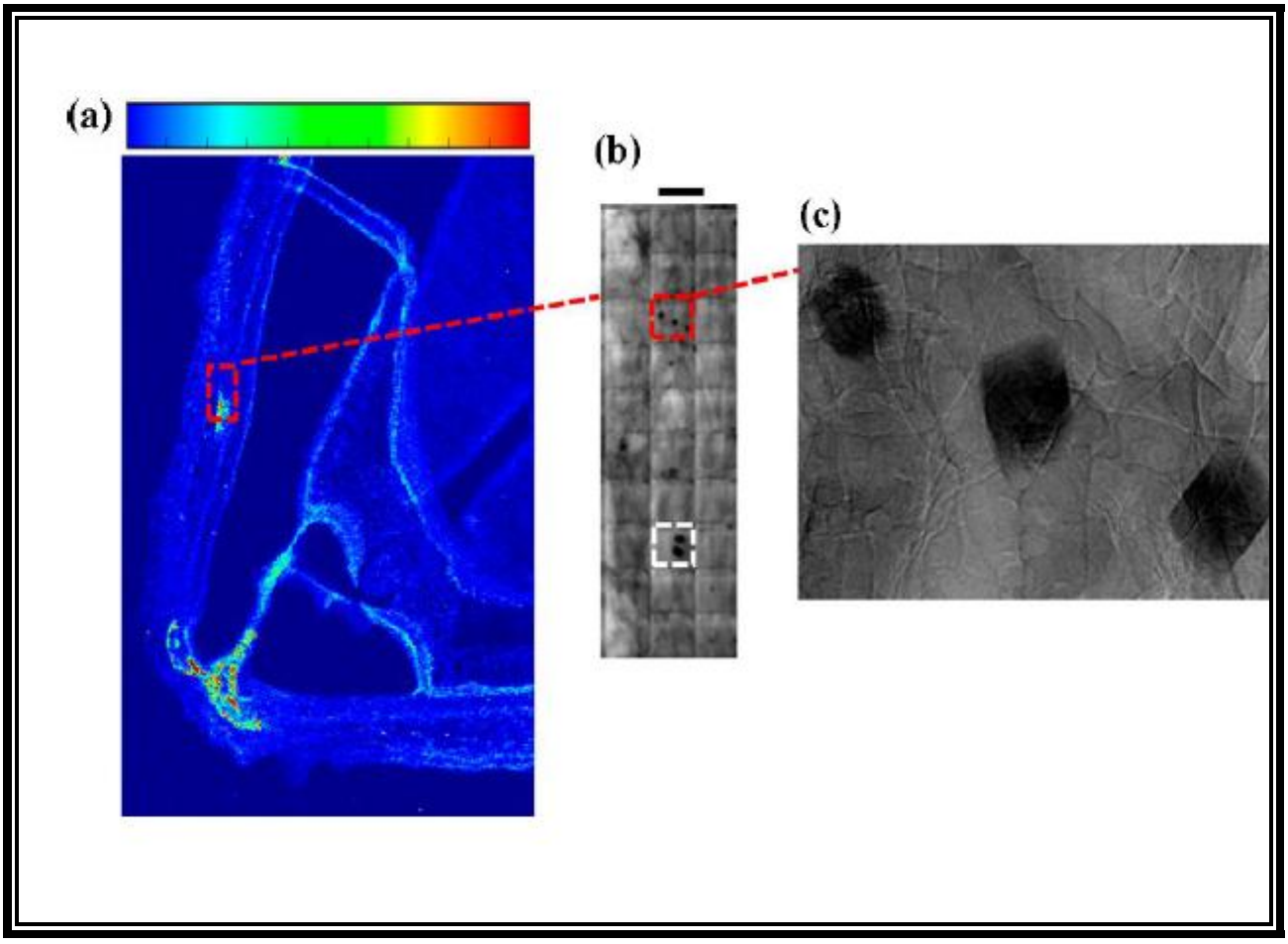

Figure 16. Images of the transversal section of a soybean pod grown in soil treated with 500 mg of ZnO/kg. (a) Zn μ-XRF map, where the red square denotes the area where TXM was performed. (b) TXM image, where the red square indicates a magnification of the area shown in (c). White square denotes the area where Zn K-edge μ-XANES were collected.

Table 3: Nitrogen fixation Potential

	Moles ethylene min^{-1} g^{-1}	Points	Avg. R^2
Control	1.97±0.99 b	5	0.96
100 mg CeO_2 Kg^{-1}	2.87±0.92 b	4-5	0.96
500 mg CeO_2 Kg^{-1}	0.39±0.09 a	5	0.99
1000 mg CeO_2 Kg^{-1}	0.28±0.16 a	4-5	0.93
50 mg ZnO Kg^{-1}	1.91±1.16 b	5	0.83
100 mg ZnO Kg^{-1}	2.55±1.16 b	5	0.97
500 mg ZnO Kg^{-1}	0.99 ±0.58 b	5	0.98

3.4 Conclusion

Key issues in studying the interaction of crop plants with NPs are the determination of their entrance in the food chain, their biotransformation, and the possible presence of the NPs or their derived products in the next plant generation. The results of this study have shown that soybean plants grown in soil impregnated with ZnO NPs did not accumulate these NPs in the grains. The XANES data suggest that the Zn accumulated in the seeds of soybean plants is linked to O, resembling the form of Zn-citrate. To our knowledge, this is the first time that the translocation of Zn from ZnO NPs in soil grown soybean pods has been reported. On the other hand, although the BCF for Ce in soybean pods was low, the LCF results suggest that most of the Ce stored in the soybean pods was in the form of CeO2 NPs. The PF results also suggest that a small percentage of the Ce in the pod could be changing its oxidation state from Ce(IV) to

Ce(III). In addition, CeO_2 nanoparticles were absorbed by the root system (root and nodule), with high concentrations of CeO_2 severely diminishing the N_2 fixation. The results of these analyses have shown that CeO_2 NPs in soil can be taken up by food crops. This suggests that CeO_2 NPs can reach the food chain and potentially reach the next soybean plant generation.

CHAPTER 4

General Conclusions

There is great concern, but little information, regarding the potential impacts of NPs to plants, agriculture and the food supply. The results of this dissertation have shown the effects of two metal oxide nanoparticles on mesquite and soybean plants. To our knowledge the use of synchrotron imaging techniques such as μXRF and μXANES to evaluate the distribution and speciation of NPs in mesquite plants was used for the first time. Our study showed no evidence of ZnO NPs in the tissues of mesquite; nevertheless high concentrations of Zn, when compared to control, were detected in the plant, suggesting the dissociation of ZnO in/on the root surface. Oscillations from the Zn spectra in the vascular area of mesquite samples suggested different coordination environments. We believe different Zn ligands such as organic acids are the basis of those oscillations since Zn is a natural micronutrient, the plant uses predetermined pathways to mobilize the Zn. Our results also showed an increase in the presence of stress enzymes; however no chlorosis, necrosis, stunting or wilting, was observed in the plant. Although insight mechanisms of the response of a plant to NPs can be obtained from hydroponic studies, such evidence is inadequate to understand how NPs will affect crops grown in NPs contaminated soil. The Soybean study presented in this dissertation was the first one which used grown plants to maturity in NP impacted soil. ICP-OES and ICP-MS data showed that soybean plants grown in organic farm soil spiked with ZnO or CeO2 NPs take up and translocate Zn and Ce throughout the plant. The μ-XRF image from the soybean stem shows that most of the Zn was found in the phloem, which is part of the vascular system of the plant. The results from μ-XANES suggest that the Zn within the soybean plant was no longer in the form of ZnO NPs. Our results also suggest that Zn(II) was associated with oxygen from organic acids. LC fitting of the μ-XANES spectra showed Zn-citrate as the closest match for the Zn found in the plant. In addition SR-TXM analysis showed Zn precipitates in the soybean pod. For the CeO2 NPs, μ-XRF imaging showed the presence of Ce in the edible part of the soybean, LC-fitting corroborated that the Ce

was coordinated as CeO2. Finally, the highest concentrations of CeO2 were found in the root and nodules of the plant. At high concentrations of CeO2 the N2 fixation potentials in the nodule decreased more than 80% relative to control. The results of these studies have shown that N2 fixation of an important leguminous crop can be affected by high CeO2 concentrations, thus affecting soil fertility. Furthermore, our results showed that CeO2 NPs in soil can be taken up by food crops. This suggests that CeO2 NPs can reach the food chain and the next soybean plant generation.

References

CHAPTER 1

1. National Nanotechnology Initiative. Accessed 2013.10 http://www.nano.gov/
2. Hood, E. Nanotechnology: Looking As We LeapEnviron Health Perspect. 2004 September; 112(13): A740–A749.
3. Roco, M.C. The long view of nanotechnology development: the National Nanotechnology Initiative at 10 years. J. Nanopart. Res. (2011) 13:427–445
4. Project on Emerging Nanotechnologies (2013). Consumer Products Inventory. Retrieved [11/2013] from http://www.nanotechproject.org/cpi
5. Kahru, A.; Dubourguier, H.C. From Ecotoxicology to Nanoecotoxicology. *Toxicology* **2010**, *269*, 105-119.
6. Xu, H.; Liu, X.; Cui, D.; Li, M.; Jiang, M.A. Novel Method for Improving the Performance of ZnO Gas Sensors. *Sens. Actuators B. Chem.* **2006**, *114*, 301-307.
7. Tam, K.H.; Djurisic, A.B.; Chan, C.M.N.; Xi, Y.Y.; Tse, C.W.; Leung, Y.H.; Chan, W.K.; Leung, F.C.C.; Au, D.W.T. Antibacterial Activity of ZnO Nanorods Prepared by a Hydrothermal Method. *Thin Solid Films* **2008**, *516*, 6167-6174.
8. Klingshirn, C. ZnO: Material, Physics and Applications. *Chem. Phys. Chem.* **2007**, *8*, 782-803.
9. Li, C.; Liang, Z.; Xiao,H.; Wu, Y.; Liu, Y. Synthesis of ZnO/Zn2SiO4/SiO2 Composite Pigments with Enhanced Reflectance and Radiation-stability under Low-energy Proton Irradiation. *Mater. Lett.* **2010**, *64*, 1972–1974.
10. Garcia, T.; Solsona, B.; Taylor, S.H. Nano-crystalline Ceria Catalysts for the Abatement of Polycyclic Aromatic Hydrocarbons. Catal. Lett. 2005, 105, 183-189.
11. Bozek, F.; Mares, J.; Bozek, M.; Huzlik, J. Emission of Particulate Matter While Applying the Envirox TM Additive. Proceedings of the 5th WSEAS International Conference on Waste Management, Water Pollution, Air Pollution, Indoor Climate. 2011, 170-175.
12. Liao, L.; Mai, H.X.; Yuan, Q.; Lu, H.B.; Li, J.C.; Liu, C.; Yan, C.H.; Shen, Z.X.; Yu, T. Single CeO2 Nanowire Gas Sensor Supported with Pt Nanocrystals: Gas Sensitivity, Surface Bond States, and Chemical Mechanism. J. Phys. Chem. C 2008, 112, 9061-9065.
13. Yabe, S.; Sato, T. Cerium Oxide for Sunscreen Cosmetics. J. Solid State Chem. 2003, 171, 7–11.
14. Currie, V. C.; Angle, J. S.; Hill, R. L. Biosolids Application to Soybeans and Effects on Input and Output of Nitrogen. Agric., Ecosyst. Environ. 2003, 97, 345–351.
15. Lee, S. H.; Lee, H. R.; Kim, Y. R.; Kim, M. K. Toxic Response of Zinc Oxide Nanoparticles in Human Epidermal Keratinocyte HaCaT Cells. Toxicol. Environ. Health Sci. 2012, 4,14–18.
16. Moos, P. J.;Olszewski, K.;Honeggar,M.; Cassidy, P.; Leachman, S.; Woessner, D.; Cutler, N. S.; Veranth, J. M. Responses of Human Cells to ZnO Nanoparticles: A Gene

Transcription Study. Metallomics 2011, 3, 1199–1211.Sargent, J.F. *Nanotechnology: A Policy Primer*. CRS Report for Congress. **2012**.

17. Lopez-Moreno, M. L.; de la Rosa, G.; Hernandez-Viezcas, J. A.; Peralta-Videa, J. R.; Gardea-Torresdey, J. L. X-ray Absorption Spectroscopy (XAS) Corroboration of the Uptake and Storage of CeO2 Nanoparticles and Assessment of Their Differential Toxicity in Four Edible Plant Species. J. Agric. Food Chem. 2010, 58, 3689–3693
18. Lee, W. M.; An, Y. J.; Yoon, H. S.; Kweon, H. S. Toxicity and Bioavailability of Copper Nanoparticles to the Terrestrial Plants Mungbean (Phaseolus radiatus) and Wheat (Triticum aestivum): Plant Agar Test for Water-Insoluble Nanoparticles. Environ. Toxicol. Chem. 2008, 27, 1915-1921.
19. de la Rosa, G.; Lopez-Moreno, M. L.; Hernandez-Viezcas, J. A.; Peralta-Videa, J. R.; Gardea-Torresdey, J. L. Toxicity and Biotransformation of ZnO Nanoparticles in the Desert Plants Prosopis juliflora-velutina, Salsola tragus and Parkinsonia florida. Int. J. Nanotechnol. 2011, 8, 492–506
20. Rico, C.; Majumdar, S.; Duarte-Gardea, M.; Peralta-Videa, J. R.; Gardea-Torresdey, J. L. Interaction of Nanoparticles with Edible Plants and Their Possible Implications in the Food Chain. J. Agric. Food Chem. 2011, 59, 3485–3498.
21. Bunker, G., 2010. Introduction to XAFS. Cambridge University Press, New York, NY.
22. Koningsberger, D.C. and Prins, P. 1988. Xray Absorption: Principles, Applications, Techniques of EXAFS, SEXAFS, and XANES, in Chemical Analysis 92, , ed., John Wiley & Sons
23. Newville, M. Fundamentals of XAFS. Consortium for Advanced Radiation Sources University of Chicago, Chicago, IL
24. Donner, E., Punshon, T., Guerinot, M., Lombi, E., 2012. Functional characterisation of metal(loid) processes in planta through the integration of synchrotron techniques and plant molecular biology. Anal. Bioanal. Chem. 402, 3287–3298.
25. Gardea-Torresdey, J.L., Peralta-Videa, J.R., de la Rosa, G., Parsons, J.G., 2005. Phytoremediation of heavy metals and study of the metal coordination by X-ray absorption spectroscopy. Coord. Chem. Rev. 249, 1797.
26. Lombi, E., Susini, J., 2009. Synchrotron-based techniques for plant and soil science: opportunities,challenges and future perspectives. Plant Soil 320, 1–35.
27. Punshon, T., Guerinot, M., Lanzirotti, A., 2009. Using synchrotron X-ray fluorescence microprobes in the study of metal homeostasis in plants. Ann. Bot. 103, 665–672.
28. Sarret, G., Pilon-Smits, E.A.H., Castillo M.H., Isaure, M.P., Zhao, F.J., Tappero, R., 2013. Use of Synchrotron-Based Techniques to Elucidate Metal Uptake and Metabolism in Plants, in: Donald, S.(Ed.), Advances in Agronomy, Academic Press, 1–82.

CHAPTER 2

1. Luna-Suárez S, Luna-Guido ML, Frias-Hernández JT, Olalde-Portugal V, Dendooven L. Soil processes as affected by replacement of natural mesquite ecosystem with maize crop. Biol Fert Soils.1998;27:274–278.
2. Choudhury S, Panda SK. Induction of oxidative stress and ultrastructural changes in moss*Taxithelium nepalense* (Schwaegr.) both under lead (Pb) and arsenic (As) phytotoxicity. Curr Sci.2004;87:342–348.
3. Lopez ML, Peralta-Videa JR, Castillo Michel H, Martinez-Martinez A, Duarte-Gardea M, Gardea-Torresdey JL. Lead toxicity in alfalfa plants exposed to phytohormones and EDTA monitored by peroxidase catalase and amylase activities. Environ Toxicol Chem. 2007;26:2717–2723.
4. Lin C, Fugetsu Y, Watari F. Studies on toxicity of multi-walled carbon nanotubes on Arabidopsis T87 suspension cells. J Hazard Mater. 2009;170:578–583.
5. Tan X, Lin C, Fugetsu B. Studies on toxicity of multi-walled carbon nanotubes on suspension rice cells. Carbon. 2009;45:3479–3487.
6. Serret G, Williams G, Isaure M-P, Marcus MA, Fakra SC, Frerot H, Pairis S, Geoffroy N, Manceau A, Saumitou-Laprade P. Zinc distribution and speciation in *Arabidopsis halleri* × *Arabidopsis lyrata*progenies presenting various zinc accumulation capacities. New Phytol. 2009;184:581–595.
7. Gallego SM, Benavides MP, Tomaro ML. Effect of heavy metal ion excess on sunflower leaves: evidence for involvement of oxidative stress. Plant Sci. 1996;121:151–159.
8. Kruger N. The Bradford Method for Protein Quantitation Department of Plant Sciences. University of Oxford; UK: 2008. The Protein Protocols Handbook.
9. Murguia I, Tarantino D, Vannini C, Bracale M, Carravieri S, Soave C. *Arabidopsis thaliana* plants overexpressing thylakoidal ascorbate peroxidase show increased resistance to paraquat-induced photooxidative stress and to nitric oxide-induced cell death. Plant J. 2004;38:940–953.
10. Marcus MA, MacDowell AA, Celeste R, Manceau A, Padmore HA, Sublett RE. Beamline 10.3.2 at ALS: a hard X-ray microprobe for environmental and material sciences. J Synchrotron Radiat.2004;11:239–247.
11. Ressler T. WinXAS: a program for X-ray absorption spectroscopy data analysis under MS-Windows.J Synchrotron Radiat. 1998;5:118–122.
12. Lopez-Moreno ML, de la Rosa G, Hernandez-Viezcas JA, Castillo-Michel H, Botez C, Peralta-Videa JR, Gardea-Torresdey JL. Evidence of the differential biotransformation of ZnO and CeO2 nanoparticles on soybean (*Glycine max*) plants. Environ Sci Technol. 2010 doi: 10.1021/es903891g.
13. Cuypers A, Vangronsveld J, Clijsters H. The redox status of plant cells (AsA and GSH) is sensitive to zinc imposed oxidative stress in roots and primary leaves of *Phaseolus vulgaris*. Plant Physiol Biochem.2001;39:657–664.

14. Chen K, Elimelech M. Aggregation and deposition kinetics of fullerene (C-60) nanoparticles.Langmuir. 2006;22:10994–11001.
15. Franklin NJ, Rogers SC, Apte GE, Batley GE, Gadd PS, Casey PS. Comparative toxicity of nanoparticulate ZnO, bulk ZnO, and ZnCl2 to a freshwater microalga (*Pseudokirchneriella subcapitata*): the importance of the particle solubility. Environ Sci Technol. 2007;41:8484–8490.
16. Rayner-Canham G. Descriptive Inorganic Chemistry. 2. Freeman; New York: 1999.
17. Salisbury FB, Ross CW. Plant Physiology. 2. Wadsworth Publishing Company; Belmont, CA: 1978.
18. Lin D, Xing B. Root uptake and phytotoxicity of ZnO nanoparticles. Environ Sci Technol.2008;42:5580–5585.
19. de la Rosa, Lopez-Moreno, Hernandez-Viezcas, Peralta-Videa, Gardea-Torresdey Toxicity and biotransformation of ZnO nanoparticles in the desert plants *Prosopis juliflora-velutina*, *Salsola tragus*and *Parkinsonia florida*. Int J Nanotechnol. in press.
20. Parsons JG, Lopez ML, Gonzalez CM, Peralta-Videa JR, Gardea-Torresdey JL. Toxicity and biotransformation of uncoated and coated nickel hydroxide nanoparticles on mesquite plants. Environ Toxicol Chem. 2009;29:1146–1154.

CHAPTER 3

1. Rico CM, Majumdar S, Duarte-Gardea M, Peralta-Videa JR, Gardea-Torresdey JL (2011) Interaction of nanoparticles with edible plants and their possible implications in the food chain. J Agric Food Chem 59:3485–3498.
2. Nowack B, et al. (2012) Potential scenarios for nanomaterial release and subsequent alteration in the environment. Environ Toxicol Chem 31:50–59
3. Kiser MA, Ryu H, Jang HY, Hristovski K, Westerhoff P (2010) Biosorption of nanoparticles to heterotrophic wastewater biomass. Water Res 44:4105–4114.
4. Limbach, L., Bereiter, R. Muller, E,. Krebs, R., Gally, R., Stark, (2008)W.J., Removal of Oxide Nanoparticles in a Model Wastewater Treatment Plant: Influence of Agglomeration and Surfactants on Clearing Efficiency. Environ. Sci. Technol. 42, 5828–5833
5. Hong, J., Peralta-Videa, J.R., Gardea-Torresdey, J.L. Nanomaterials in Agricultural Production: Benefits and Possible Threats? ustainable Nanotechnology and the Environment: Advances and Achievements. Chapter 5, pp 73–90. DOI: 10.1021/bk-2013-1124.ch005
6. Economic Research Service, United States Department of Agriculture. Briefing Room: Soybeans and Oil Crops. Background, 2012. Available at http://www.ers.usda.gov/topics/crops/soybeans-oil-crops.aspx. Accessed October 16, 2013.

7. Food and Agriculture Organization of the United Nations. http://faostat.fao.org/site/339/default.aspx. Accessed October 16, 2013
8. Lopez-Moreno, M. L.; de la Rosa, G.; Hernandez-Viezcas, J. A.; Castillo-Michel, H.; Botez, C.; Peralta-Videa, J. R.; Gardea-Torresdey, J. L. Evidence of the Differential Biotransformation and Genotoxicity of ZnO and CeO2 Nanoparticles on Soybean (Glycine max) Plants. Environ. Sci. Technol. 2010, 44, 7315–7320
9. Castillo-Michel, H.; Hernandez-Viezcas, J. A.; Servin, A. D.; Peralta-Videa, J. R.; Gardea -Torresdey, J. L. Arsenic Localization and Speciation in the Root-Soil Interface of the Desert Plant Prosopis juliflora-velutina. Appl. Spectrosc. 2012, 6, 719–727.
10. Serret, G.; Williams, G.; Isaure, M.-P.; Marcus, M. A.; Fakra, S. C.; Frerot, H.; Pairis, S.; Geoffroy, N.; Manceau, A.; Saumitou-Laprade, P. Zinc Distribution and Speciation in Arabidopsishalleri, Arabidopsis lyrata Progenies Presenting Various Zinc Accumulation Capacities. New Phytol. 2009, 184, 581–595.
11. Zhao, L.; Peralta-Videa, J. R.; Varela-Ramirez, A.; Castillo-Michel, H.; Li, C.; Zhang, J.; Aguilera, R.; Keller, A.; Gardea-Torresdey, J. L. Effect of Surface Coating and Organic Matter on the Uptake of CeO2 NPs by Corn Plants Grown in Soil: Insight into the Uptake Mechanism. J. Hazard. Mater. 2012, 225-226, 131–138.
12. Roggenbuck, J.; Waitz, T.; Wagner, T.; Lotz, A.; Fröba, M.; Tiemann, M. Ce LIII-XANES Investigation of Nanoporous CeO2. HASYLAB-Jahresbericht HASYLAB/DESY, Hamburg, 2007, 461-462.
13. Keller, A. A.; Wang, H.; Zhou, D.; Lenihan, G. C.; Miller, C. R.; Ji, Z. Stability and Aggregation of Metal Oxide Nanoparticles in Natural Aqueous Matrices. Environ. Sci. Technol. 2010, 44, 1962–1967.
14. Priester, J. H.; Ge, Y.; Mielke, R.; Horst, A. M.; Cole Moritz, S.; Espinosa, K.; Gelb, J.; Walker, S. L.; Nisbet, R. M.; An, Y. J.; et al. Soybean Susceptibility to Manufactured Nanomaterials with Evidence for Food Quality and Soil Fertility Interruption. Proc. Natl. Acad. Sci. U.S.A. www.pnas.org/cgi/doi/10.1073/pnas.1205431109.
15. Weaver RW, Danso SKA (1994) Dinitrogen Fixation. Methods of Soil Analysis Part 2-Microbiological and Biochemical Properties, eds Weaver RW, Angle JS, Bottomley PS (Soil Science Society of America, Madison, WI), pp 1019–1045.
16. Packer AP, et al. (2007) Validation of an inductively coupled plasma mass spectrometry (ICP-MS) method for the determination of cerium, strontium, and titanium in ceramic materials used in radiological dispersal devices (RDDs). Anal. Chim. Acta 588:166–172
17. Solé, V. A.; Papillon, E.; Cotte, M.; Walter, P.; Susini, J. A Multiplatform Code for the Analysis of Energy-Dispersive X-ray Fluorescence Spectra. Spectrochim. Acta 2007, 62, 63–68.
18. Ravel, B.; Newville, M. Athena, Artemis, Hephaestus: Data Analysis for X-ray Absorption Spectroscopy Using IFEFFIT. J. Synchrotron Radiat. 2005, 12, 537–541.

19. Nachimuthu, P.; Shih, W.; Liu, R.; Jang, L.; Chen, J. The Study of Nanocrystalline Cerium Oxide by X-ray Absorption Spectroscopy. J. Solid State Chem. 2000, 149, 408–413.
20. Webb, S. M. The MicroAnalysis Toolkit: X-ray Fluorescence Image Processing Software. AIP Conf. Proc. 2011, 1365,19610.1063/1.3625338.
Webb, S. M. SixPACK: A Graphical User Interface for XAS Analysis Using IFEFFIT. Phys. Scr. 2005, T115, 1011–1014.
21. Lopez-Moreno, M. L.; de la Rosa, G.; Hernandez-Viezcas, J. A.; Peralta-Videa, J. R.; Gardea-Torresdey, J. L. X-ray Absorption Spectroscopy (XAS) Corroboration of the Uptake and Storage of CeO2 Nanoparticles and Assessment of Their Differential Toxicity in Four Edible Plant Species. J. Agric. Food Chem. 2010, 58, 3689–3693
22. Riesen, O.; Feller, U. Redistribution of Nickel, Cobalt, Manganese, Zinc, and Cadmium via the Phloem in Young and Maturing Wheat. J. Plant Nutr. 2005, 28, 421–430.
23. Kopittke, P. M.; Menzies, N. W.; de Jonge, M. D.; McKenna, B. A.; Donner, E.; Webb, R. I.; Paterson, D. J.; Howard, D. L.; Ryan, C. G.; Glover, C. J.; et al. In Situ Distribution an Speciation of Toxic Copper, Nickel and Zinc in Hydrated Roots of Cowpea. J. Plant Physiol. 2011, 156, 663–673.
24. Thangavel, P.; Long, S.; Minocha, R. Changes in Phytochelatins and Their Biosynthetic Intermediates in Red Spruce (Picea rubens Sarg.) Cell Suspension Cultures under Cadmium and Zinc Stress. Plant Cell, Tissue Organ Cult. 2007, 88, 201–216.
25. Lombi, E.; de Jonge, M. D.; Donner, E.; Kopittke, P. M.; Howard, D. L.; Kirkham, R.; Ryan, C. G.; Paterson, D. Fast X-ray FluorescenceMicrotomography of Hydrated Biological Samples. PLoS One 2011, 6, e20626.
26. Hurrell, R. F.; Juillerat, M. A.; Reddy, M. B.; Lynch, S. R.; Dassenko, S. A.; Cook, J. D. Soy Protein, Phytate, and Iron Absorption in Humans. Am. J. Clin. Nutr. 1992, 56, 573–578.
27. Chen YX, et al. (2003) Effect of cadmium on nodulation and N2-fixation of soybean in contaminated soils. Chemosphere 50:781–787.

Vita

Jose Angel Hernandez-Viezcas has a bachelor in Chemical Engineering and a M.S. in Environmental Sciences. In 2010 he joined the doctoral program in Chemistry at The University of Texas at El Paso. During his time at UTEP he received fellowships from the University of California-Center for Environmental Implications of Nanotechnology and from the National Council for Science and Technology (Mexico). During his doctoral studies Mr. Hernandez-Viezcas published 20 peer reviewed journals and presented his work in national and international meetings, while working in Dr. Gardea-Torresday laboratory. His dissertation, Determination of the effects of ZnO and CeO2 nanoparticles in Mesquite (Prosopis juliflora velutina) and Soybean (Glycine max): Synchrotron and Spectroscopic approaches was presented in the fall of 2013. Dr. Hernandez-Viezcas will join and FDA founded post doctoral position at the Connecticut experimental research station in New Heaven, CT.

Permanent address: 4111 westcity ct apt 212
El Paso, TX, 79902

This thesis/dissertation was typed by the author